PROGRESS REPORT NO. 2

SARA Projects

Integrated Seismic Risk Assessment in South America (SARA): the hazard component

Topic 3:

Modeling the subduction process along the western coast and creation of a source model to be used for hazard calculations

PROGRESS REPORT

2015, March

Prepared by

Elkin De Jesús Salcedo Hurtado, Ph. D
Department of Geography, Universidad del Valle - Cali, Colombia

Carlos Alberto Vargas Jiménez, Ph. D
Department of Geosciences, Universidad Nacional de Colombia - Bogotá, Colombia

Marily Triviño Abella, M. Sc. Candidate
Department of Geosciences, Universidad Nacional de Colombia - Bogotá, Colombia

With the administrative assistance of the
FUNDACIÓN UNIVERSIDAD DEL VALLE

Introduction

The Global Earthquake Model (GEM) promotes the improvement of public understanding of seismic risk based on three disciplinary areas: hazard, physical risk, and social vulnerability and integrated risk. Historically there are almost 77,000 lives, 15 million people affected and USD 37bn economic losses - this is the earthquake toll in South America for the last 40 years (Swis Re and GEM, 2014), then as part of this initiative, the Seismic Risk in South America (SARA) project has into its aims to calculate hazard and risk, and to estimate the compounding social and economic factors that increase the physical damage and decrease the post-event capacities of populations to respond to and recover from damaging earthquake events in South America. So, the first module is based in the building a seismic hazard model for the region for which it is necessary to establish a characterization and modelling of subduction process as source model for calculating of seismic hazard model.

Seismotectonic region in South America is characterized by convergence between Caribbean, Nazca and Cocos oceanic plates and South American lithospheric Plate, this arc extends on the one hand along the western coast of South America from southern Patagonian mountains to its intersection with Panama and on the other hand the Northern boundary with Caribbean Plate. However, with purposes for obtaining a better analysis, we have included seismicity and seismotectonic along Caribbean and Mesoamerican plates (Figure 1). Thus, convergence between subducting Nazca plate beneath the South American, Mesoamerican and Caribbean plates are responsible of a constrasting stress regimen and deformation which is supported by a broad variety of tectonic settings related to the Andes range uplifting, presence of volcanism, large suture zones, wide foothills and foreland basins, etc. (Bilek, 2009; Rhea *et al.*, 2010; Chen *et al.*, 2001).

Since 1900 to 2012 near to 67000 events have been registered along the study zone, and almost 35% correspond to shallow seismicity related to possible orogenic processes and typical crustal deformation, while the other 75% correspond to earthquakes located in subduction zones that highlights the permanent slab slipping along the dip interface between 35 km and 700 km, and with magnitudes that reach Mw 8.4.

This work presents a new segmentation model of subduction geometry in the study are a based on different sort of data sets along the western margin of the South American continent. This work presents new estimations of several variables that improving the knowledge of seismic sources along subduction zones as part of the an integral hazard model leadership by the GEM´s program (Cardona *et al*., 2005; Corredor, 2003; Holt *et al*., 1991;Vergnolle *et al*., 2010). We develop our proposal by using statistical analysis of a representative instrumental catalogue of seismicity, application of declustering algorithms,, estimation of parameters of frequency - magnitude distribution, as well as incorporing new calculations of seismotectonic deformation from focal mechanism solutions and crustal strain rate analysed from GPS measurements.

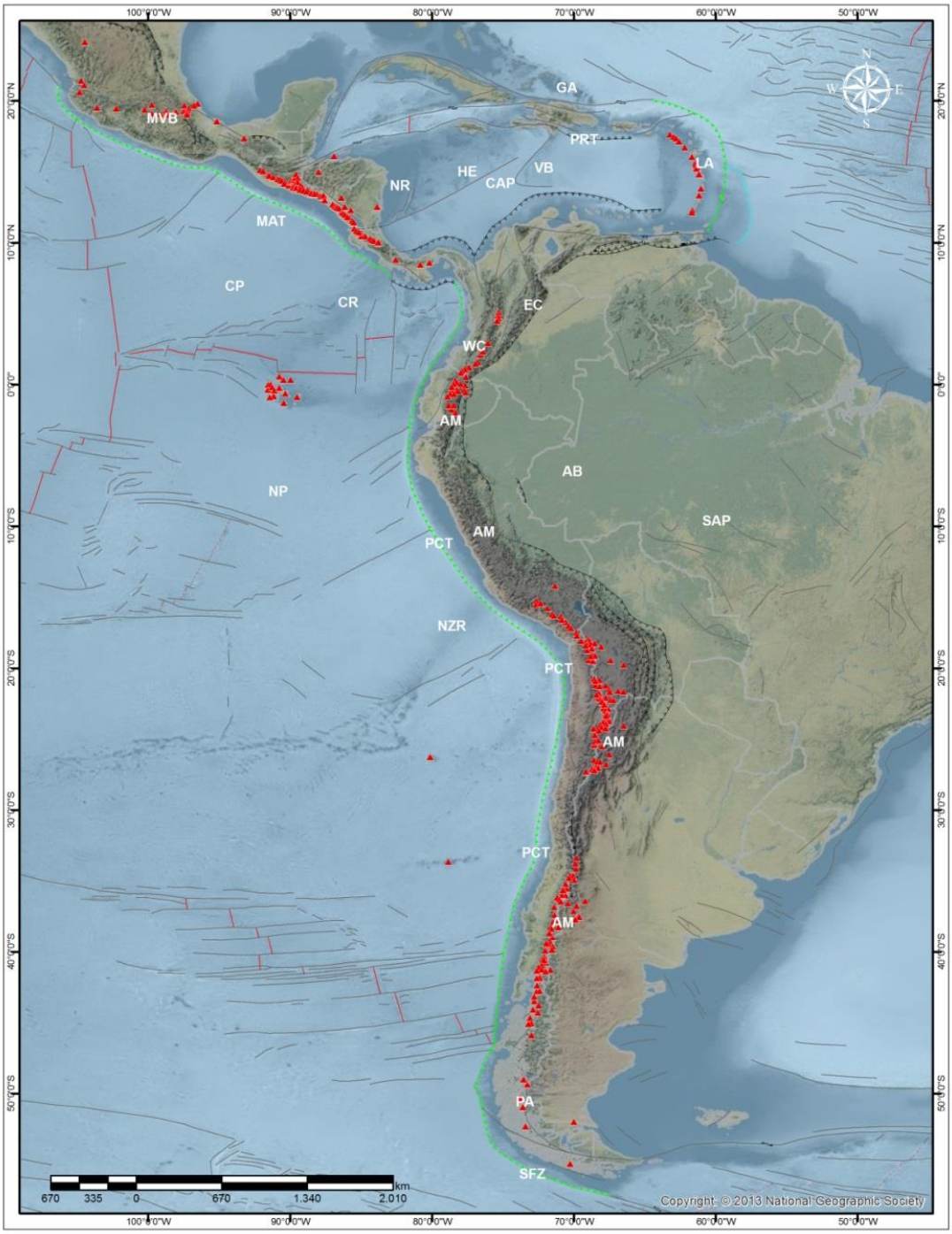

Figure 1. Map with delimitation of study area and geotectonic characterization, include the main structural features and volcanism. WC: Western Cordillera; CC: Central Cordillera; EA: Eastern Cordillera; VB: Venezuela Basin; CAP: Caribbean Plate; MVB: Mexican volcanic belt; HE: Hess Escarpment; NR: Nicaragua Rise; NZR: Nazca Ridge; MAT: Middle America Trench; CP: Cocos Plate; NP: N Nazca Plate; SAP: South American Plate; GA: Greater Antilles; LA: Lesser Antilles; PCT: Peru-Chile Trench; AM: Andes Mountains; AB: Amazonas Basin; PA: Patagonia Andean; SFZ: Shackleton Fracture Zone

Geotectonic Framework

The South American backbone is mainly composed of metamorphic and igneous complexes of Archean/Proterozoic age and was consolidated during late Proterozoic to Early Paleozoic times in contrast to the Patagonian Platform which mainly evolved during the early Paleozoic, and has been tecntono-thermally active up to the Cenozoic. The hightest non-collisional mountain range of the world, the Andes, was developed on the western continental margin of the plate, at least from the early Paleozoictime, and its evolution continues until today with active vulcanism and seismicity due to continuous subduction of Pacific plates beneath the South American Plate and in the northern areas by a complex relay of subduction processes with the Caribbean plate. Therefore, the South American plate reveals a long and complex geologic history. Early theories about the Eastern margin of the South American plate indicated that it forms a more than 10000 km long divergent margin, which developed as a result of the separation of the South American plate and the African plate since Mesozoic through the opening of the South Athlantic and the break-up of Gondwana. Recent studies suggest than the estimated horizontal forces arising from the South American plate no wadays are in the same order of magnitude as the forces (10^{13} $Nm^{-1)}$ required to initiate subduction at a passive margin (Marques *et al*., 2013).

Several authors have analysed the Andes and proposed different geological classifications in order to identify discrete segments with somewhat homogeneous geological properties. The inherited geological history, as well as the present tectonic setting, is responsible for the unique geology of the Northern, Central, and Southern Andes. The Northern Andes are the result of Mesozoic and Cenozoic collisions of oceanic terranes, prior to the present Andean-type setting. The Central Andes have a long history of subduction and volcanic arc activity, while the Southern Andes record the closing of a back-arc oceanic basin, and almost no volcanic arc activity. These major geological units have along-strike variations in the subduction geometry that controls the different volcanic zones (Ramos, 1999).

Hence, South American continent can be regarded as a fusion of several Precambrian terrains, fold belts, and intracratonic sedimentary basins to the East, a late Proterozoic block to the South and two Phanerozic orogenic zones to the West (The Andes) and north (Caribbean) bordering the continent. Then, 14 main geological provinces have been defined by Almeida *et al*., (2000) and Van der *et al*., (2013) as follow: Guyana shield, Solimões basin, Amazonas basin, Parnaíba basin, São Francisco craton, Brazilian shield, Paraná basin, Chaco basin, Guyana basin, Andean foreland basins, Amilina province, Patagonia province, West–central Cordillera, and Andean province.

Geometry of the Subduction Process

The subduction of an oceanic lithospheric plate under the continent is a complex process of plate interactions that involve a broad sort of rocks, ages, angles, velocities, etc. Nevertheless, there is some consensus that the main parameters that control the geometry, coupling and tectonic setting of Andean-type subduction zone are: length of the Benioff zone, relative convergence rate, age of the down going slab, slab-dip, direction of mantle flow, absolute motion of the over-riding plate and slab retreat.

Historically a large variety of tectonic settings in subduction zones have been defined. These tectonic regimes can be addressed through the structural style in the overriding plate, which is determined by its stress state. In the study area, have been described several segments with contrasting subduction parameters. Table 1 shows these segments suggested by selected authors:

Table 1. Subduction segments reported in previous studies

Author	Class Number	Subduction Zones
Mpodozis and Ramos, 1990	3 Segments	• Tarapacá (21°-27°S lat) • Central Chile Basin (288–358S lat.) • Rocas Verdes Basin
Ramos and Folguera, 2009	4 Subtypes, 11 Segments	Present flat-slab segments: • Pampean • Peruvian • Bucaramanga
		Incipient flat-slab segments: • Carnegie • Guanacos • Tehuantepec
		Three older and no longer active Cenozoic flat-slab segments: • Altiplano • Puna • Payenia
		Inferred Palaeozoic flat slab segments: • Early Permian • San Rafael
Ramos, 2009	4 Great Segments	• Nicaragua • Sandwich • Oregon • Chile
Gutscher *et al*., 2000	10 segments	• Chile (28°-33°S) • Peru (2°-15°S) • Ecuador (1°S – 2°N) • Colombia (6° - 9°N) • Costa Rica (82° - 84°W) • México (96° - 100°W) • Cascadia (46° - 49°N)

		• Alaska (145° - 150°W) • SW Japan (132° - 137°E) • New Guinea (136° - 142°E)

Seismicity and great earthquakes

Seismology provides information about seismic sources, the structure of the earth, and the relation of earthquakes with the tectonic processes that produce them (Stein and Wysession, 2013). Distribution of earthquakes provides strong evidence for the idea of essentially rigid plates, with deformation concentrated on their boundaries. Hence, earthquakes primarily occur at the boundary where the ~100 km – thick tectonic plates converge, diverge, or slide apart each other (Stein and Wysession, 2013).

Almost the entire length of the convergent South American margin has ruptured several times in the past few centuries, as detailed in historical accounts that date back to the 1500s, for that reason, it is necessary to identify better subduction zone segments potentiality dominated by relatively long recurrence times of giant earthquakes (Müller and Landgrebe, 2012). Several authors have already provided rupture descriptions and historical accounts for events occurred before of 1900s (Bilek, 2009).

Data

With the purpose of build an integral model of subduction geometry we have integrated analyses of different variables supported on a geospatial information database collected specifically for this work. Seismic dataset includes a review of three earthquake catalogues (Table 2, Figure 2a) and selection of the best one for achieving the most representative register of the seismotectonic settings in the region.

Table 2. . Characteristics of the catalogues reviewed in this work

Catalogue	No. of Events	Period	Type of Magnitudes	Analysis applied
USGS	119581	1905 – 2015	Mw, Ms, Mb, Ml	Evaluation of data
ISC EHB Bulletin	13586	1960 – 2008	Mw	Evaluation of data
ISC – GEM Bulletin	190518	1905 - 2012	Mw, Ms, Mb, Ml	• Selection of events into preview delimitation of subduction zone • Selection of events with magnitude type: Mw, Mb, Ms • Convertion to Moment Magnitude (Mw) from Global expressions proposed by ISC-GEM Catalogue. • Select events with Depth >= 35 km • Reject of events with fixed depth and depth major to 35 km.

Focal mechanism solutions were obtained from ISC dataset, which includes information for overall 8165 records between 1977 and 2012 about Dip, Strike, Rake angles, Magnitude, Depth, latitude and longitude parameters. This dataset was used for estimating seismotectonic deformation (Figure 2b).

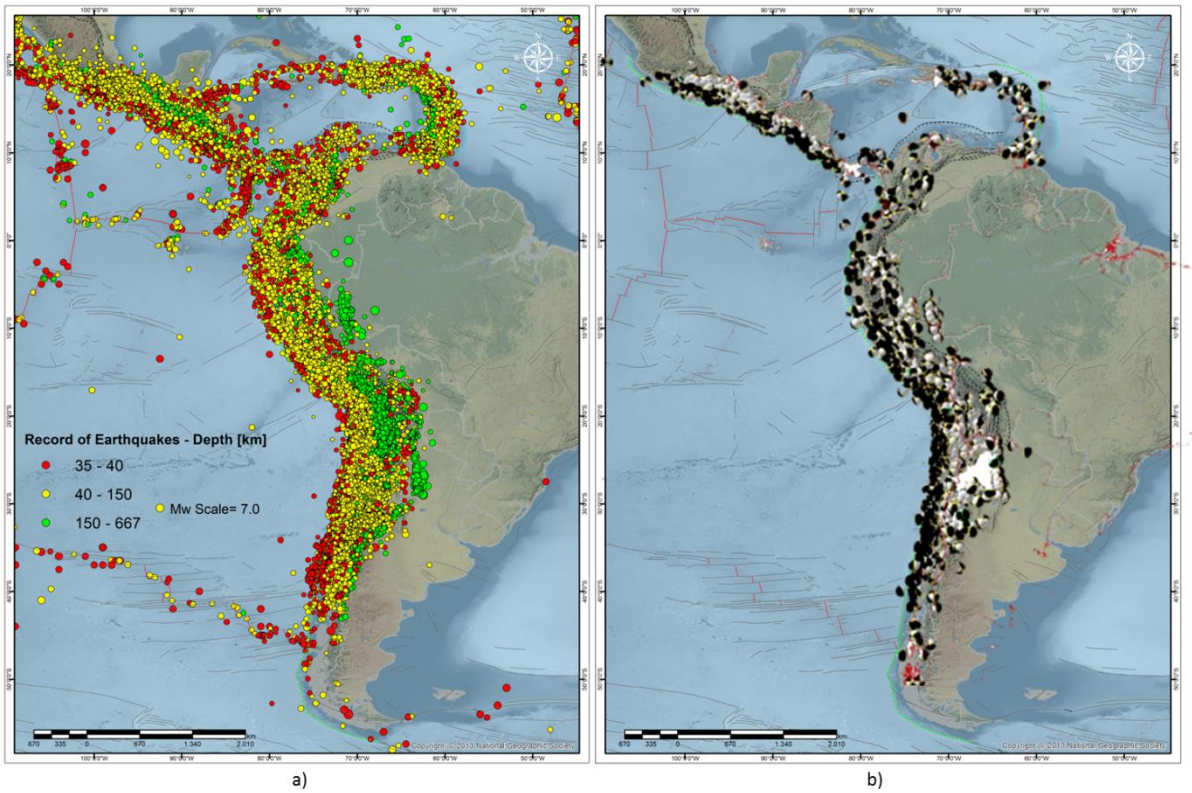

Figure 2.a) Seismic events characterized by their depth in the study area; b) Beach balls symbol corresponds to focal mechanism solution of the seismic events with Depth major to 35 km.

A database with weekly solutions of velocity displacement in three components for GNSS SIRGAS-CON network of continuous operation was gotten together with theoretical VEMOS model. This data complement analyses if the displacement rate of crust in South American continent and boundary plates (Figure 3).

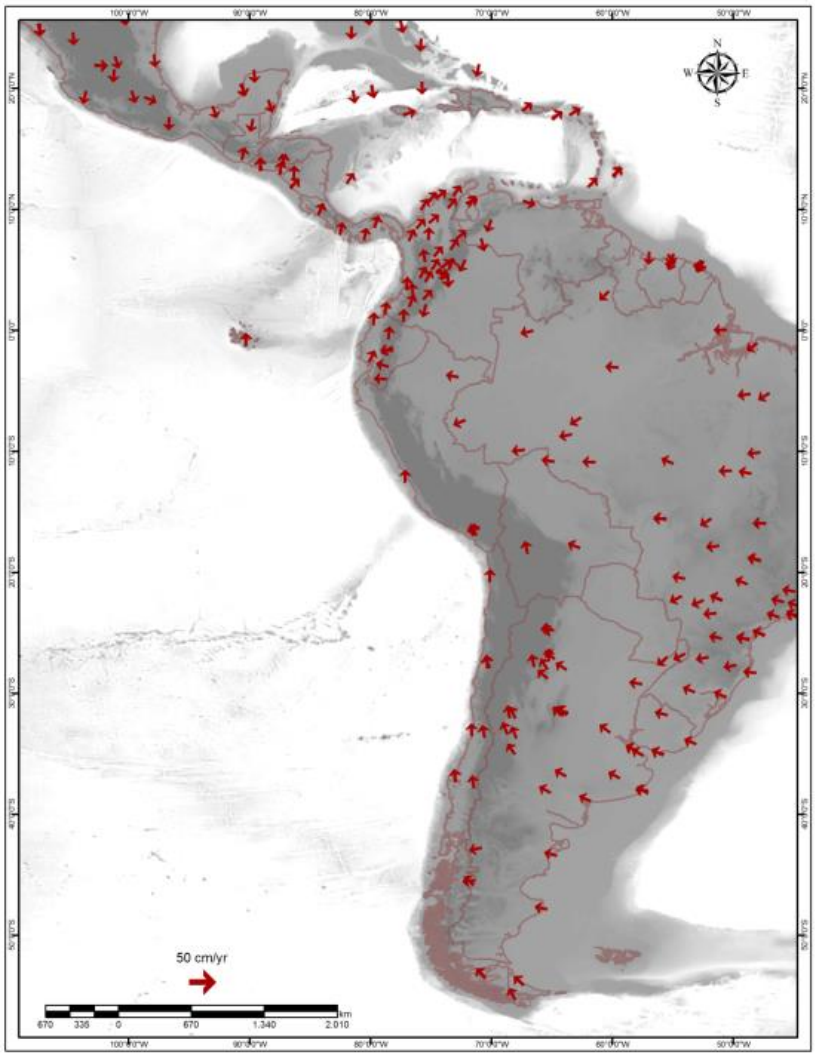

Figure 3. Map with horizontal displacement rates obtained from GPS measurements on GNSS Network - SIRGAS-CON (Sanchez and Seitz, 2011).

Geology and Tectonic data include layers of Geology, faults and volcanoes in scales that ranging between 1:50.000.000 and 1:25.000.000 for South American, Centro American and Caribbean regions.

Other geophysical variables used in this works are: gravity anomaly, earth magnetic anomaly, data of P-wave perturbations derived from regional tomographies and stress field map coming from the World Stress Map. All this material has been down load from official institutions webpage, while Heat Flow dataset was proved by main researcher. Table 3 presents a summary of data source collected by categories and used in this work:

Table 3. Main variables used along this study

Data Type	Data Subset	Source of Data
Seismology	Earthquake Catalogue (1900-2014)	USGS/NEIC (PDE) catalogue (http://neic.usgs.gov)
	Earthquake Catalogue (1900-2012)	• ISC EHB Bulletin - International Seismological Centre, EHB Bulletin, http://www.isc.ac.uk, Internatl. Seis. Cent., Thatcham, United Kingdom, 2010. • ISC Bulletin - International Seismological Centre, On-line Bulletin, http://www.isc.ac.uk, Internatl. Seis. Cent., Thatcham, United Kingdom, 2010.
	Catalogue of Focal Mechanism (1900-2012)	(ISC-CMT)
Geology and Tectonic	Geological Map of the World - Scale 1:50.000.000 (2009): Geology, structure, Volcanoes	Commission for the Geological Map of the World (CCMW)
	Geologic Map of South America - Scala 1:25.000.000 (2010).	Commission for the Geological Map of the World (CCMW)
	Geologic Map of Caribbean- Scala 1:25.000.000	United States Geological Service (USGS)
Gephysics	GravityAnomaly	Sandwell_Smith_18.1
	EMAG2: A 2-arc-minute resolution Earth Magnetic Anomaly	EMAG2: A 2-arc-minute resolution Earth Magnetic Anomaly
	HeatFlow	J.H. Davies and D. R. Davies (2010) - Earth's surface heat flux
	Tomography of P wave speed	Li, C., R. D. van der Hilst, E. R. Engdahl, and S. Burdick (2008), A new global model for P wave speed variations in Earth's mantle, Geochem. Geophys. Geosyst, 9, Q05018, doi:10.1029/2007GC001806.
	World Stress Map - WSM (2008) Smoothed	Heidbach, O., Tingay, M., Barth, A., Reinecker, J., Kurfeß, D., Müller, B., The World Stress Map based on the database release 2008, equatorial scale 1:46,000,000, Commission for the Geological Map of the World, Paris, doi:10.1594/GFZ.WSM.Map2009, 2009.
Geodesy	Horizontal and Vertical Velocity of Displacement	SIRGAS (VEMOS Model 2009) and Sánchez, L., M. Seitz (2011). Recent activities of the IGS Regional Network Associate Analysis Centre for SIRGAS (IGS RNAAC SIR). DGFI Report No. 87. Munich SIRGAS-CON)

METHOD

Analysis of seismicity

After selection of data included in ISC Bulletin according with criteria showed above, we proceeded to do the next filters:

- Selection of events into preview delimitation of subduction zone
- Select events with Depth >= 35 km
- Reject of events with fixed depth
- Selection of events with magnitude type: Mw, Mb, Ms
- Conversion to Moment Magnitude (Mw)

Formulas for homogenization of magnitude coming from global expressions proposed by ISC-GEM catalogue (Storchak *et al*, 2012; International Seismological Center, 2010) (Figure 4).

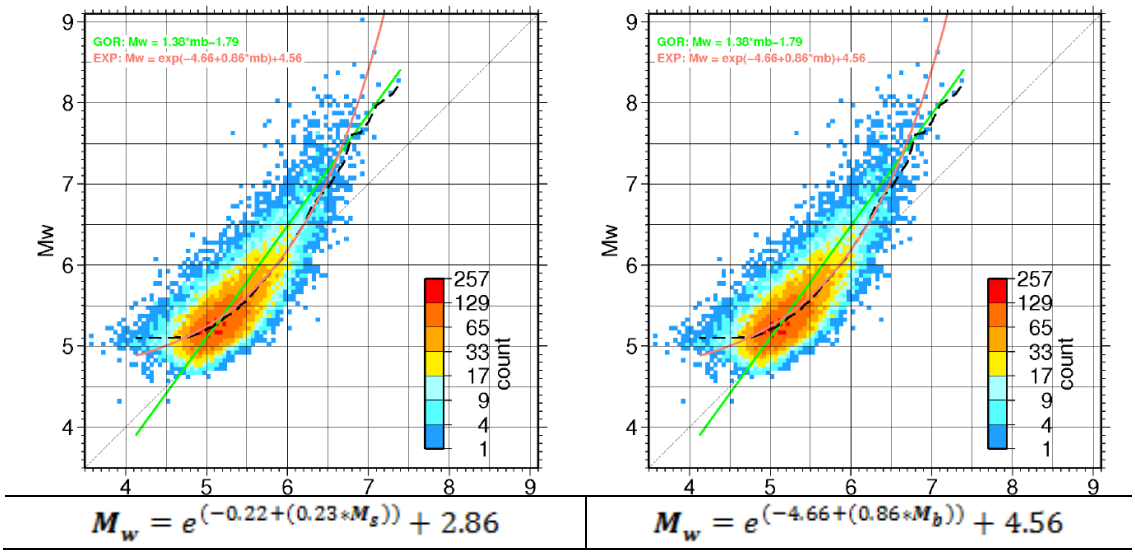

Figure 4. Formulas derived from global ISC-GEM studies and used in this work.

A catalogue with 43727 seismic events registered in Central and South America between 1904 and 2012 was obtained, with magnitudes (Mw) ranging between 2.1 and 8.4 and depths between 35 and 700 km, which were analysed through different statistical tools (Zuñiga *et al*., 2005). Next steps describe how was processed this dataset

1. *Catalogue data through time:* Graphics of cumulative number of events respect time were made. On base of Figure 5, it is evident a change on the earthquake

activity since 1970. Our dataset considers information previous to 1970, and consequently this small amount of events impact the frequency of large events.

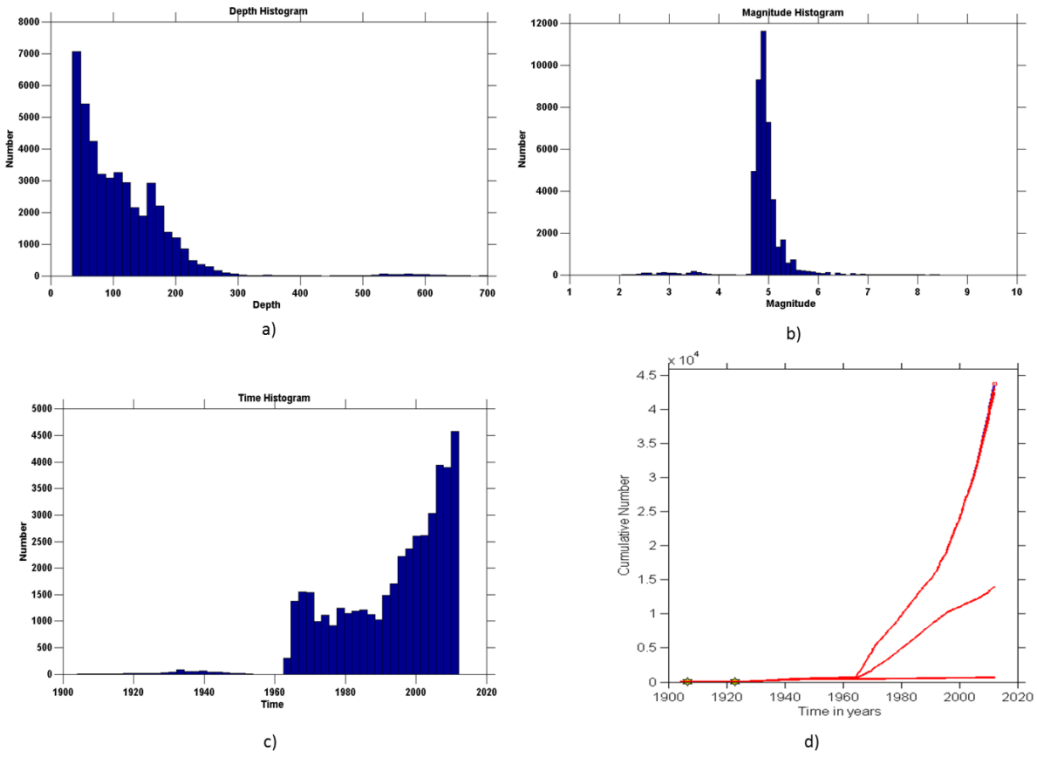

Figure 5. Characteristics Catalogue at time. a) Depth Histogram. b) Magnitude Histogram. c) Time Histogram. d) Cumulative Number Curve

2. *Declustering:* Separation of dependent and independent seismicity was made, identifying the main shocks through Reasenberg (1985), Uhrhammer (1986), Gruenthal and Gardner & Knopoff (1974) algorithms (Hainzl *et al*.,2009; Van Stiphout *et al*., 2012), which were evaluated and the last one was selected for applying and using predefined windows in space and time. Then, a catalogue with 13651 earthquakes was obtained. A comparative graphics that relate time, distance and magnitude with different algorithms is presented in Figures 6a-c and Figures 7a-b.

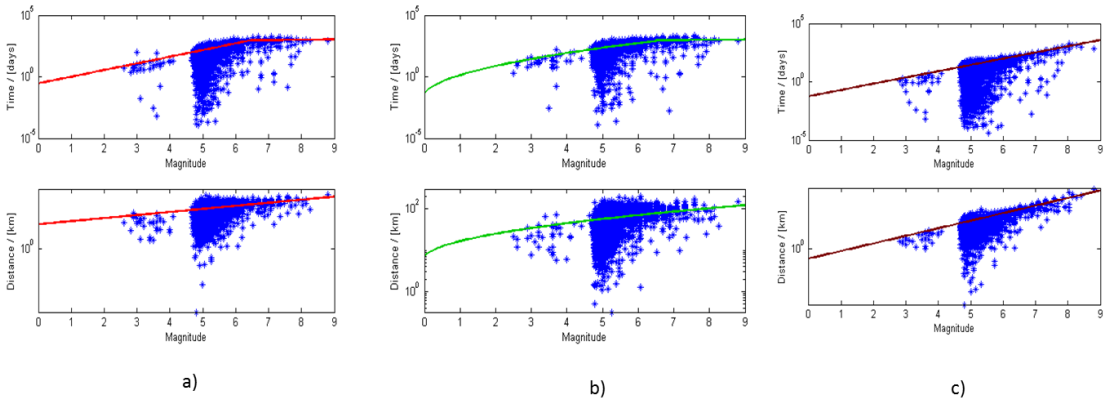

Figure 6. Declustering process based on time, space and magnitude parameters. Methods applied were: a) Gardner Knopoff Method b) Gruenthal Method c) Hurhammer Method

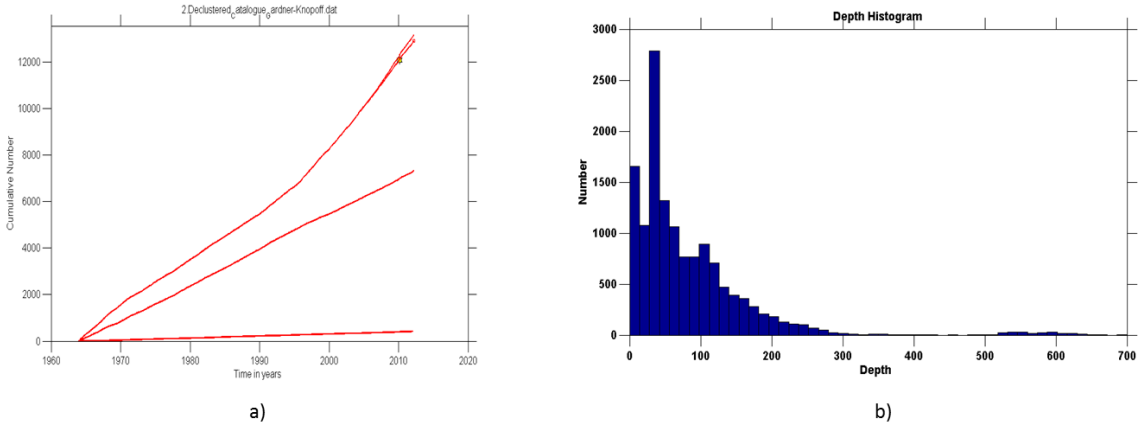

Figure 7.a) Cumulative Number Curve of events for: All, >3, >4, >5, >6 based on Gardner-Knopoff method. b) Depth Histogram based on Gardner Knoff method.

3. Calculating of Completeness Magnitude:

a) Change rates of magnitude: In this step we calculated curves of cumulative number of earthquakes for different magnitude cuts with an increment of 0.5. Thus, significative changes of magnitude were found along the historical record in the catalogue as is shown in Figure 8a-c.

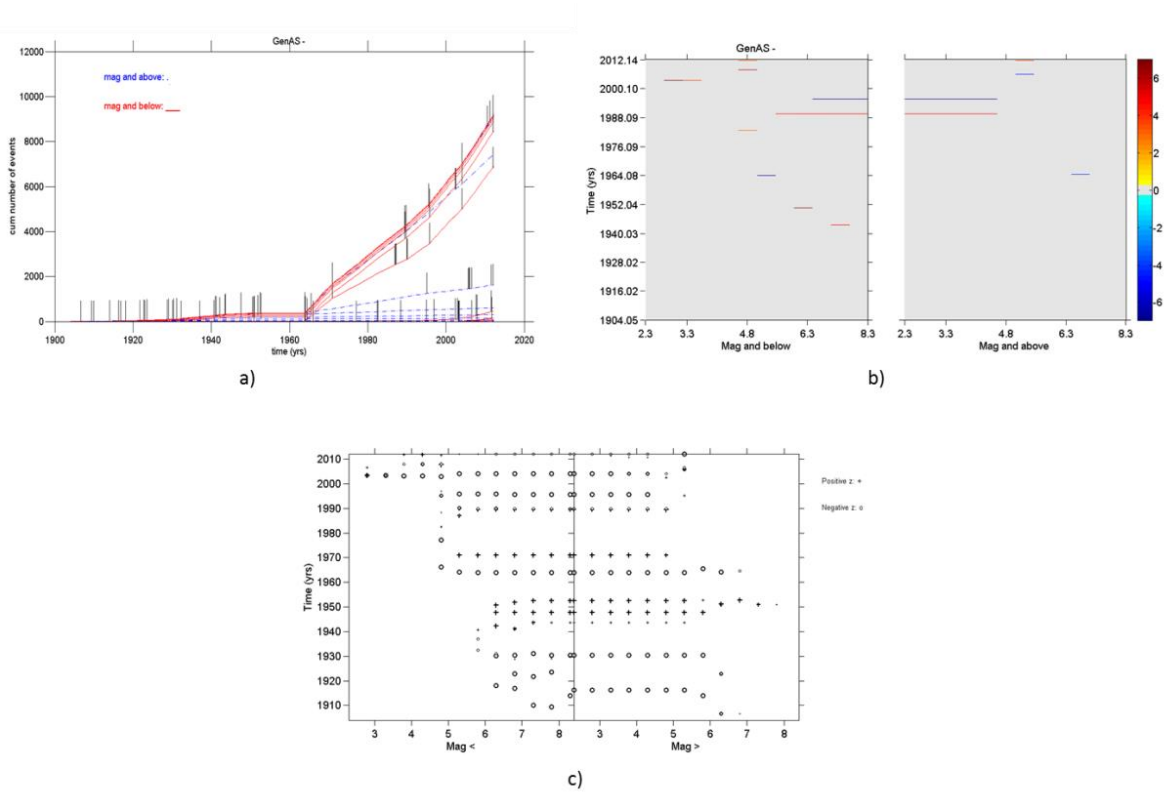

Figure 8. Change rates of magnitude of catalogue Data

These results suggest contrasting instrumental behaviour of the seismological networks with at least three specific periods: 1904-1970, 1970-1989 and 1989-2012.

b) Comparison of seismicity rates throughout different intervals of time: Based on the above ranges defined, comparison over completeness magnitude was made in order to define capabilities of detection of local and regional earthquakes (Figures 9a-c).

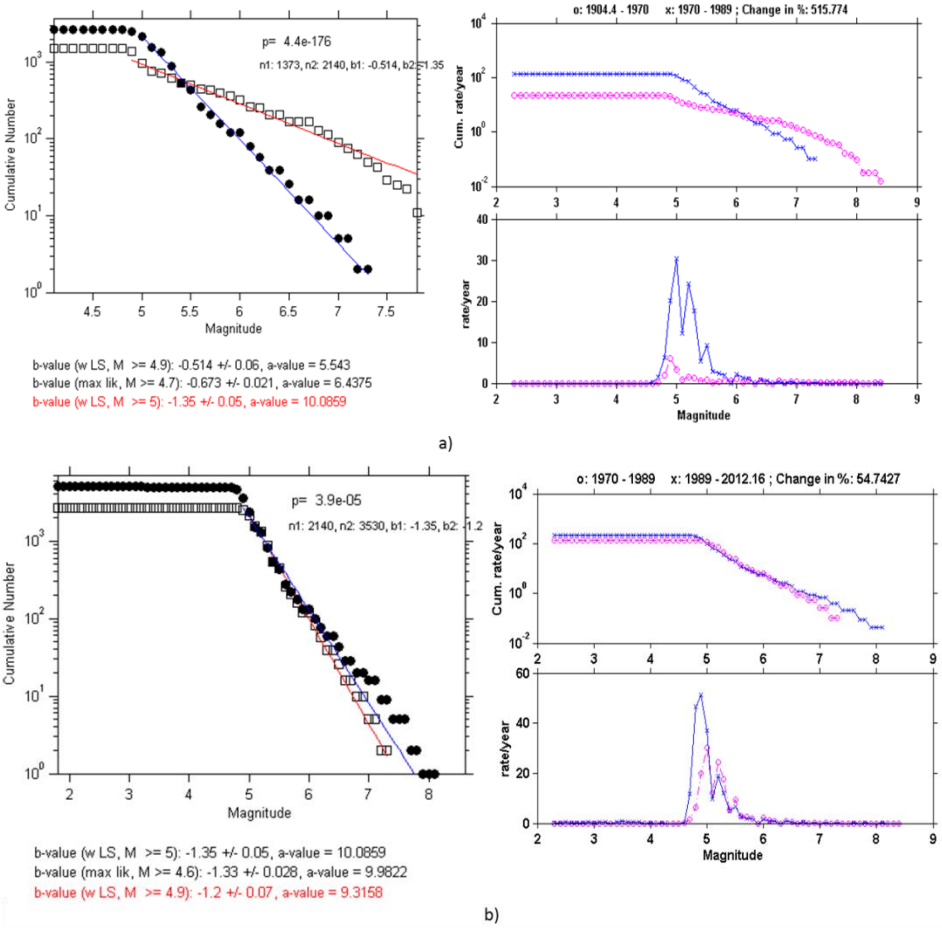

Figure 9. Comparison of seismicity rates throughout different intervals of time. a) 1904-1970 b) 1970-1987, and c) 1987-2012

After these analyses, in this work we are assuming the maximum completeness magnitude (Mc) for all period that comprising the dataset (1904 and 2012) because there are not large contrasting in these values.

A best fit of the Guthenberg-Richter relation was done for describing the frecuency-magnitude distribution of earthquakes. In Figure 10 are showed results for a, b and Mc parameters for the entire catalogue, estimated by the Maximum Likelihood approach.

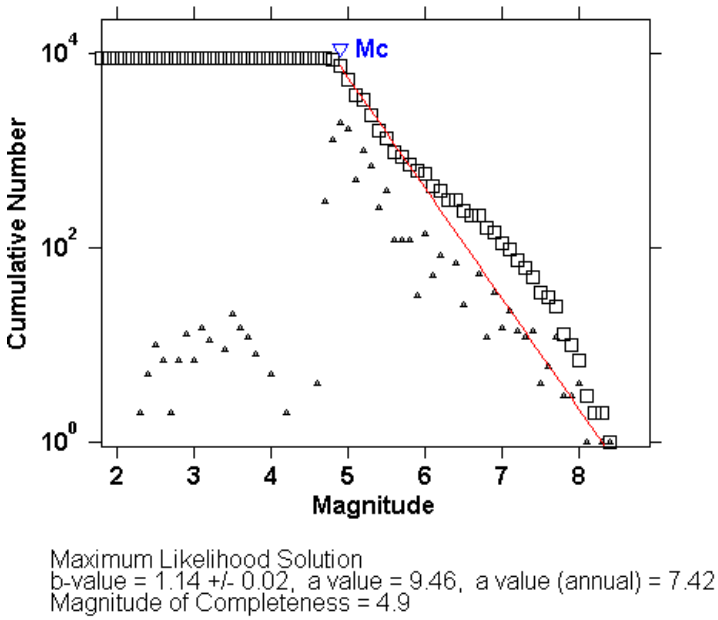

Figure 10. Frequency - Magnitude plot for all earthquakes with depth higher that 35km. Squares indicate cumulative curve for the number of earthquakes per year and triangles show incremental values. Red line is a trace of the logarithm of the numbers of earthquakes in function of magnitude give (Mw), where b-value correspond to slope and a-value is the cut point associated to maximum magnitude expected.

Analysis of Seismotectonic Deformation and Crustal Strain Rate

Focal mechanisms solutions were used for estimating the seismotectonic deformation rate (see e.g. Salazar and Vargas, 2015). Parameters as scalar moments, moment tensor components, nodal planes, principal axes and the hypocenter parameters are used for estimating effective displacements along the lithospheric profile where seismicity is available. These results were compared with data of displacement velocity derived from GPS measurements during the time window between 2000 and 2011 by the SIRGAS GPS network. Also, a multi-year solution with coordinates and velocities for each station was used as input data in the Crustal Strain Rate (CSR) model (Teza *et al.*, 2008) in order to estimate the strains using the modified least squares method (Shen *et al.*, 1996) on the nodes of a regular planar grid defined in a regular grid of 2° x 2° into study zone. These deformation estimations are keystone for supporting any sort of segmentation of the subduction geometry along the study zone.

Results

Frequency – Magnitude Distribution

Frequency-Magnitude Distribution (FMD) allowed to estimates maps for a, b and Mc parameters along a regular grid of 0.2° x 0.2° with their respective uncertainties (Figures 11a-c). The most significant parameter, the b-value, suggests a contrasting distribution of regions that refers to a subduction zone with relevant heterogeneity. Variation of the b-value parameter is ranging between 0.6 and 1.8. In this work we have classified areas based on four intervals: <0.9, 0.9-1.3, 1.3-1.7 and >1.7.

Higher interval are present in regions with major number of events release throughout several mechanisms, among them volcanoes along active magmatic belts, thrusting faulting in some foothills, some strike-slip systems and subduction zones. Lower values are present more frequently along the subduction zones. This distribution matches well with the a-value, and both define several well defined zones from Caribbean to Patagonia (Figures 11a-b).

Spatial variations of Mc (Figure 11c) are in the range between 4.8 and 5.2. Major values are located in the Middle American Trench (MAT) and the Pacific Trench (PCT), especially in regions of volcanic gaps along to AM, while zones with great seismic activity present lower value of Mc.

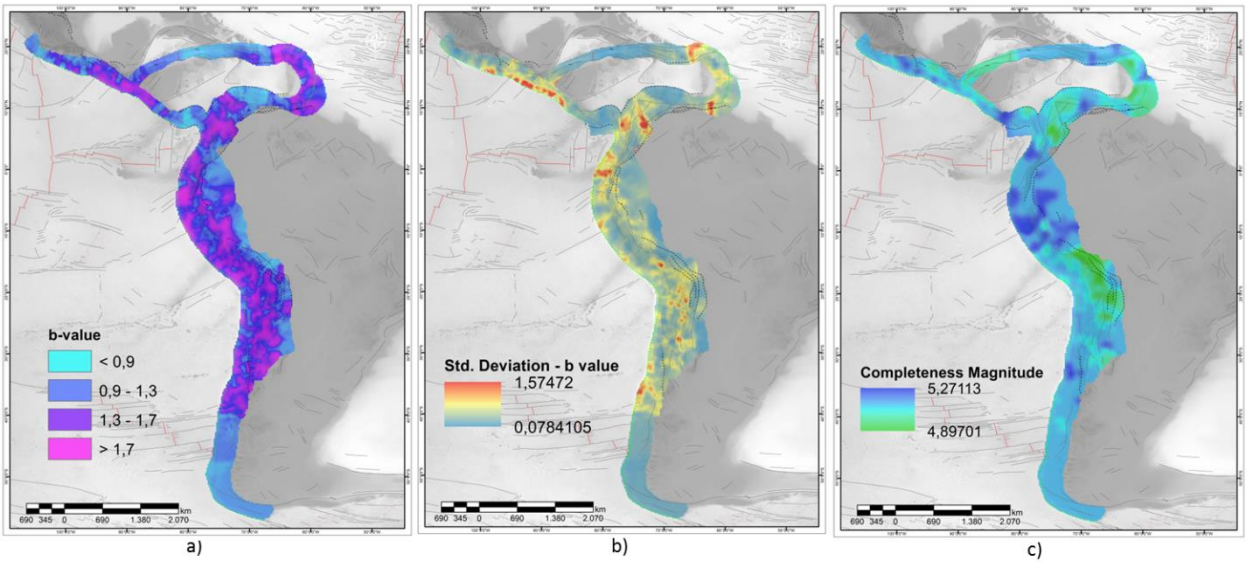

Figure 11. Results of FMD for study zone. a) Map of b-value, b) Map of Standard Deviations c) Map of Completeness Magnitude (Mc)

Seismotectonic Deformation (DST) and GNSS measurements

Higher magnitudes are suitable for the seismotectonic deformation estimations, and consequently our estimations offer a better image along the plate borders. Along five layers (0-40 km, 40-80 km, 80-120 km, 120-160 km and 160-200 km) are presented the results of this analysis (Figures 12a-e). Upper layers are supported with denser information; mean while deeper layers contain empty areas due to few data available. Figure 12a makes a comparison between rates of horizontal displacement obtained from GPS measurements and horizontal velocity of STD in depth from 0 to 40 km. It is observed that in some regions display vectors with a trend in direction similar to GPS vectors. A particular case of contrasting results between both techniques is presented in the Caribbean plate, where it does not present similar behavior in both datasets, probably due to the quite different behavior of micro plates. GPS measurements indicate a dynamic of the Northwest region of South America and Panama arc with similar orientation respect to STD vectors. STD vectors located along Peru and Ecuador toward south to beginning of PA show the highest magnitude. It is noted that GPS data have been collected onshore for which is not comparable with STD vectors on trench zones.

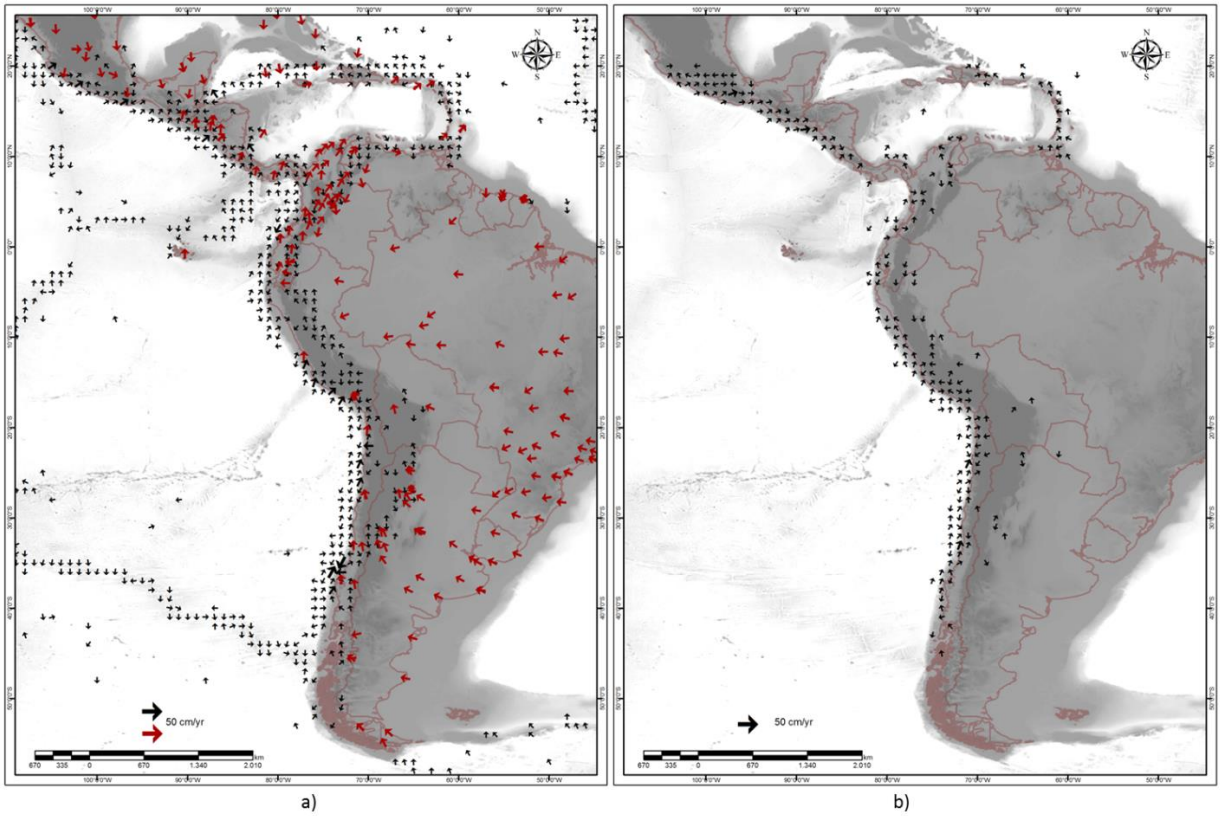

a) b)

Figures 12b to 12e show the behavior of STD vectors from 40 km to 200 km, suggesting reduction of records in depth of there is not data of seismic events for that zone. Based on a general overview of this variable, is possible consider than large mobility of plates and blocks involve large deformation zones with different mobility patterns.

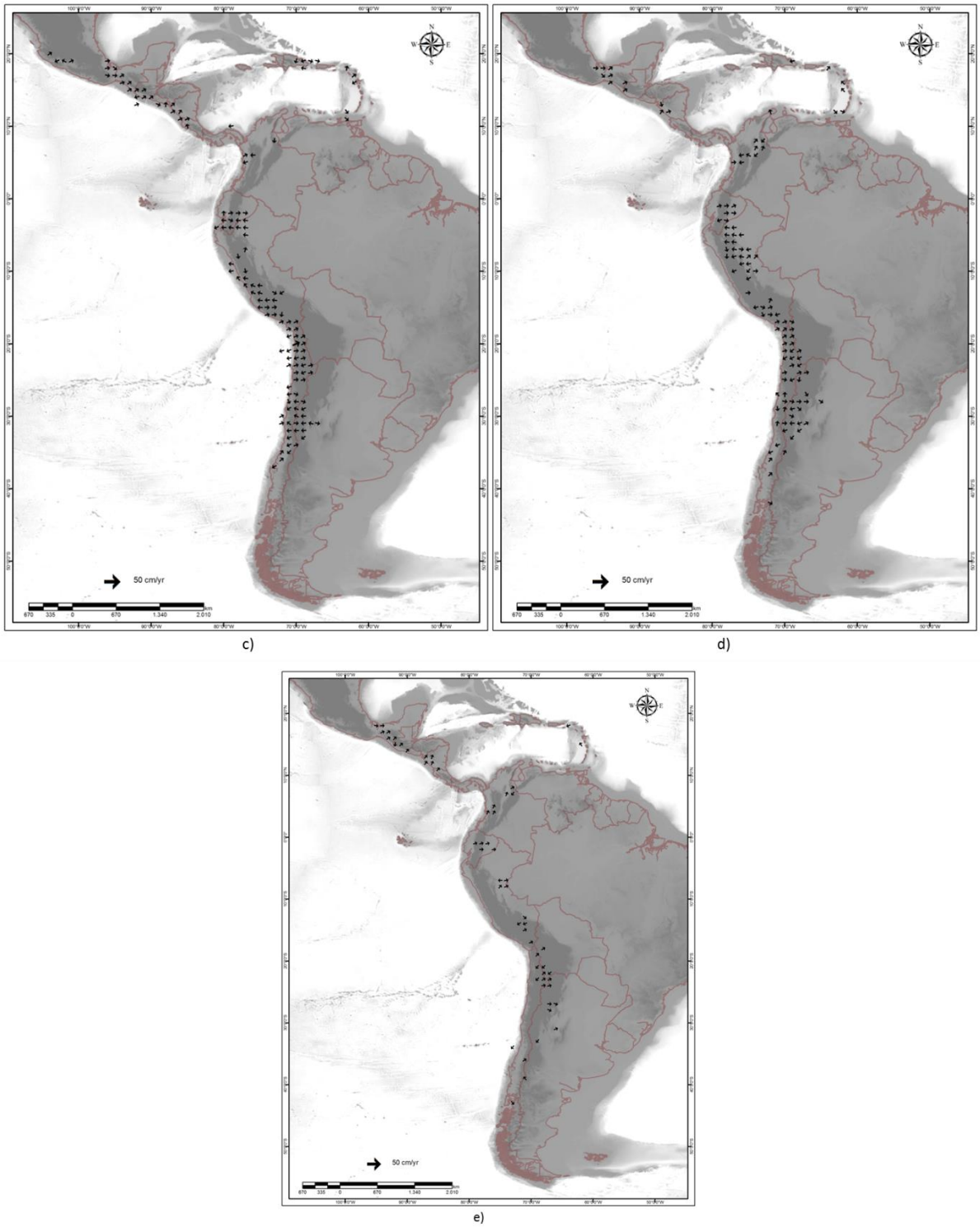

Figure 12. Horizontal velocity of Seismotectonic Deformation by focal mechanisms solutions (black arrows) in the depth range: a) Between 0 km and 40 km; b) Between 40 km and 80 km, c) Between 80 km and 120 km, d) Between 120 km and 160 km and e) Between 160 km and 200 km.

Crustal Strain Rate

GNSS measurements allowed apply the method exposed in Shen *et al.* (1996) for estimating CSR vectors (Figure 13), which indicate percent of unit strain in the time as magnitude, and direction of maximum and minimum strain. Results show a trend of maximum CSR in perpendicular direction in relation with convergence zone among tectonic plates, while minimum CSR is in the same direction to subduction zones (MAT and PCT).

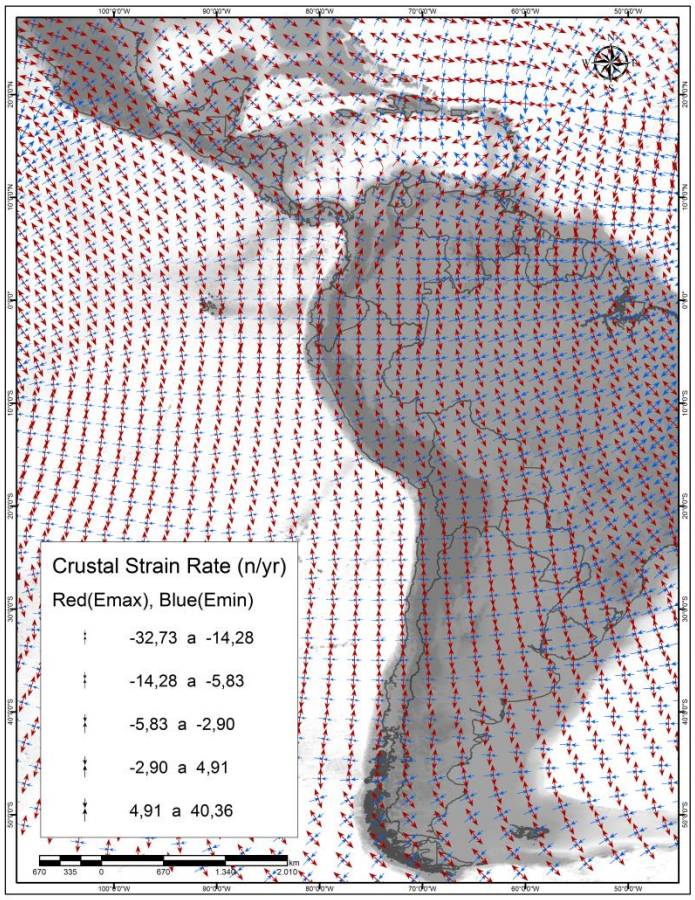

Figure 13. Vectors of Crustal Strain Rate (CSR). Red arrows indicate the maximum strains and blue arrows the minimum strains.

Discussion

Throughout an interactive process have been adjusted different variables with the purpose of define zones of similar seismic hazard behaviour along the subduction regions under South American and Caribbean. Main tectonic features and the distribution of active volcanism were also taken in account for defining segments of flat or normal type of subduction.

In addition, analysis of seismicity from statistical approaches associated with frequency – magnitude distribution of earthquakes have been considered for supporting segmentation proposal. Other relevant information in this process was topography, bathymetry and lithological age data reported in literature (Gutscher *et al*., 2000; Chen, 2001; Marques *et al*., 2013; Ramos, 2009; Müller and Landgrebe, 2012).

A total of 21 blocks are suggested in this study (Figures 14a-b).

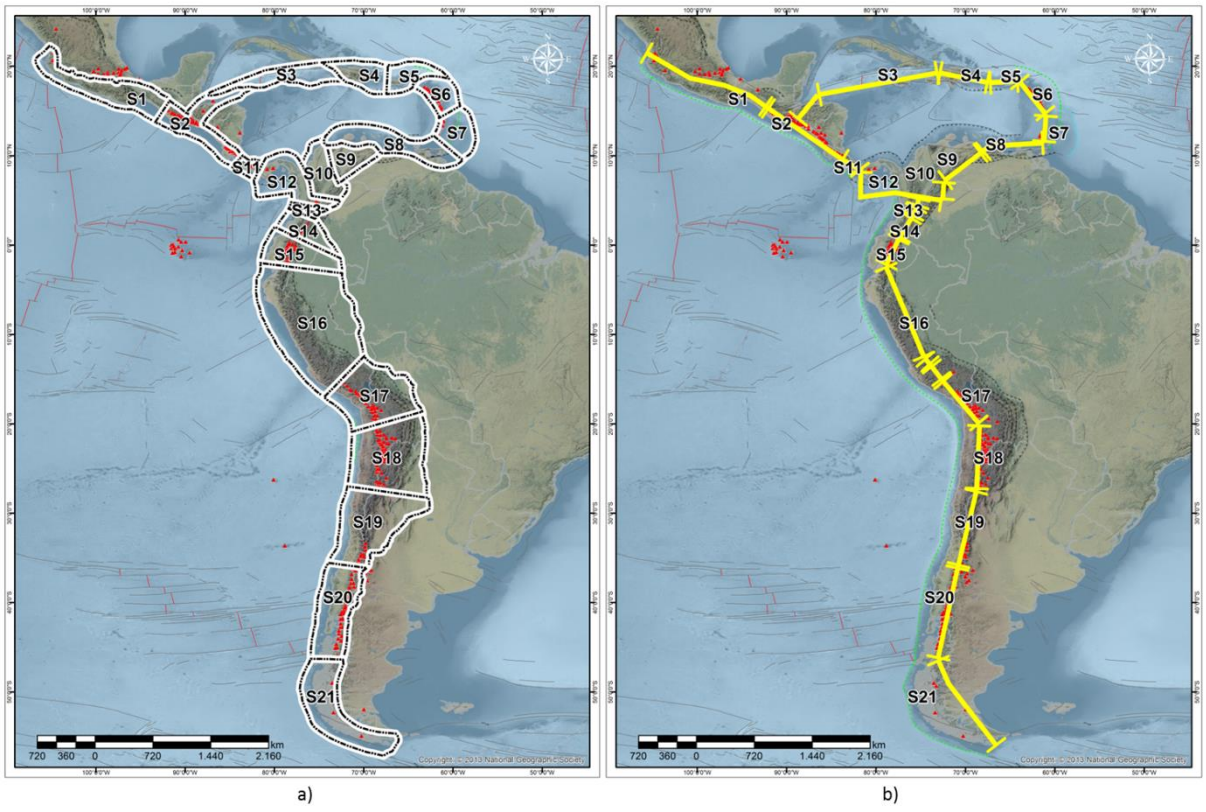

Figure 14. Map of zoning of subduction processes proposal for SA and CAP. a) Polygon zoning. b) Line zoning

Blocks have been subjected to a comparative analysis of crustal strain rates calculated based on surficial GPS measurements and constrained with seismotectonic deformation and distribution of seismicity. Figures 15 to Figure 35 support description of each block based on

distribution of events in depth, estimations of STD for each range of depth (0-40 km, 40-80 km, 80-120 km, 120-160 km and 160-200 m), and rose diagrams with direction distribution of STD by depth and block.

Block 1

Located in Northwestern extreme of convergence margin into study zone, it extends between latitudes 22°N to 15°N and longitudes 92°30'W to 106°W and covers Mexican Volcanic Belt in México Country.

Inside this block the larger seismic activity is located in the interval from 35 to 40km depth (Figure 15a), where is found out the highest rate of STD (Figure 15b). Figure 15c shows a horizontal movement along the direction ranging between 30° and 60° for all ranges of depth with exception of the range 120-160km, where velocity vector of STD varies from 60° to 90°.

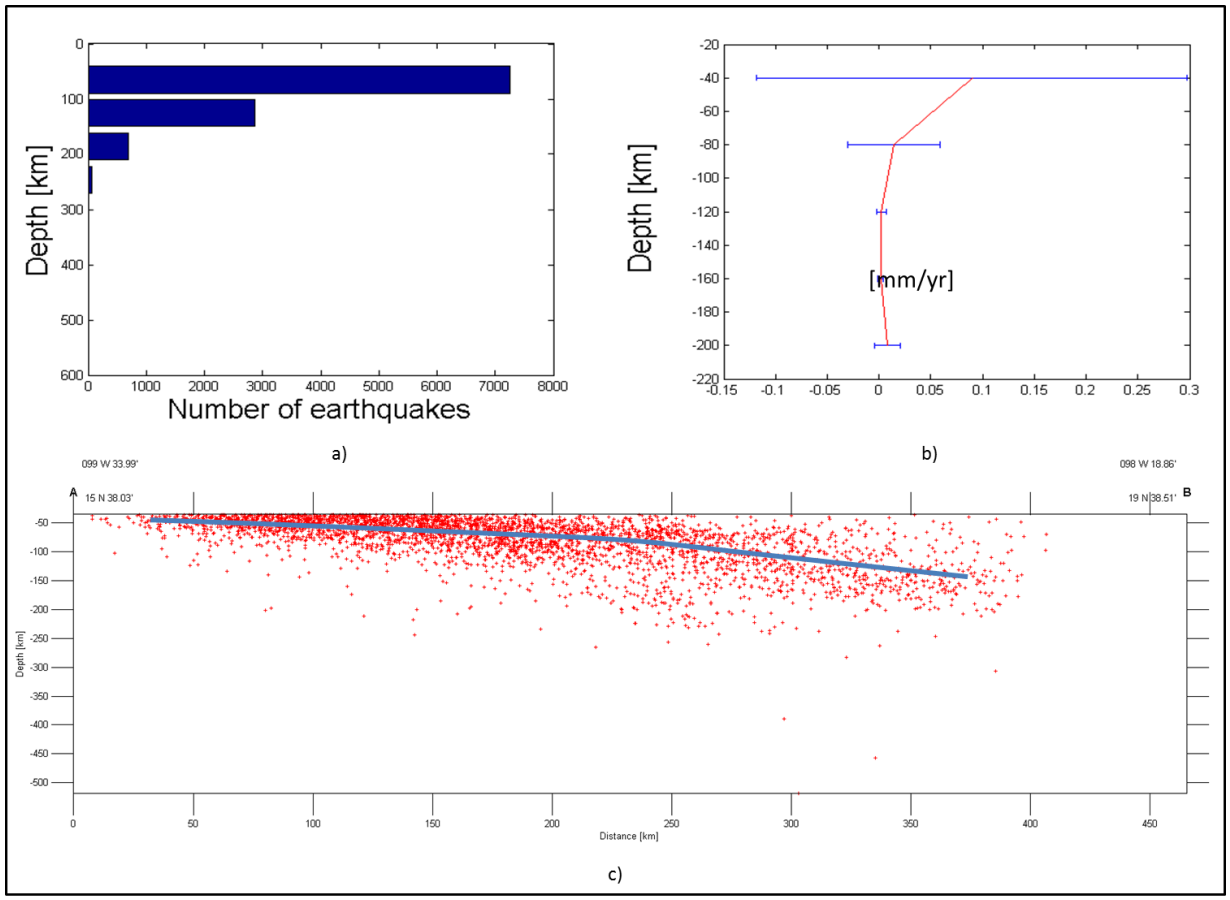

Figure 15. Block No. 1 a) Histogram of events, b) Horizontal Velocity of STD, c) Cross section of seismicity

Block 2

Block 2 encompasses the subduction zone related with the volcanic range of Guatemala and the Salvador and delineates the North westerner portion of the CAP (Figures 14 and 16).

Seismic activity is located in the depth interval 35 - 80km (Figure 16a), where is registered the highest picks of STD (Figure 16b). Figure 17c shows a preferential direction of the horizontal movement between 30° and 60° for every depth range.

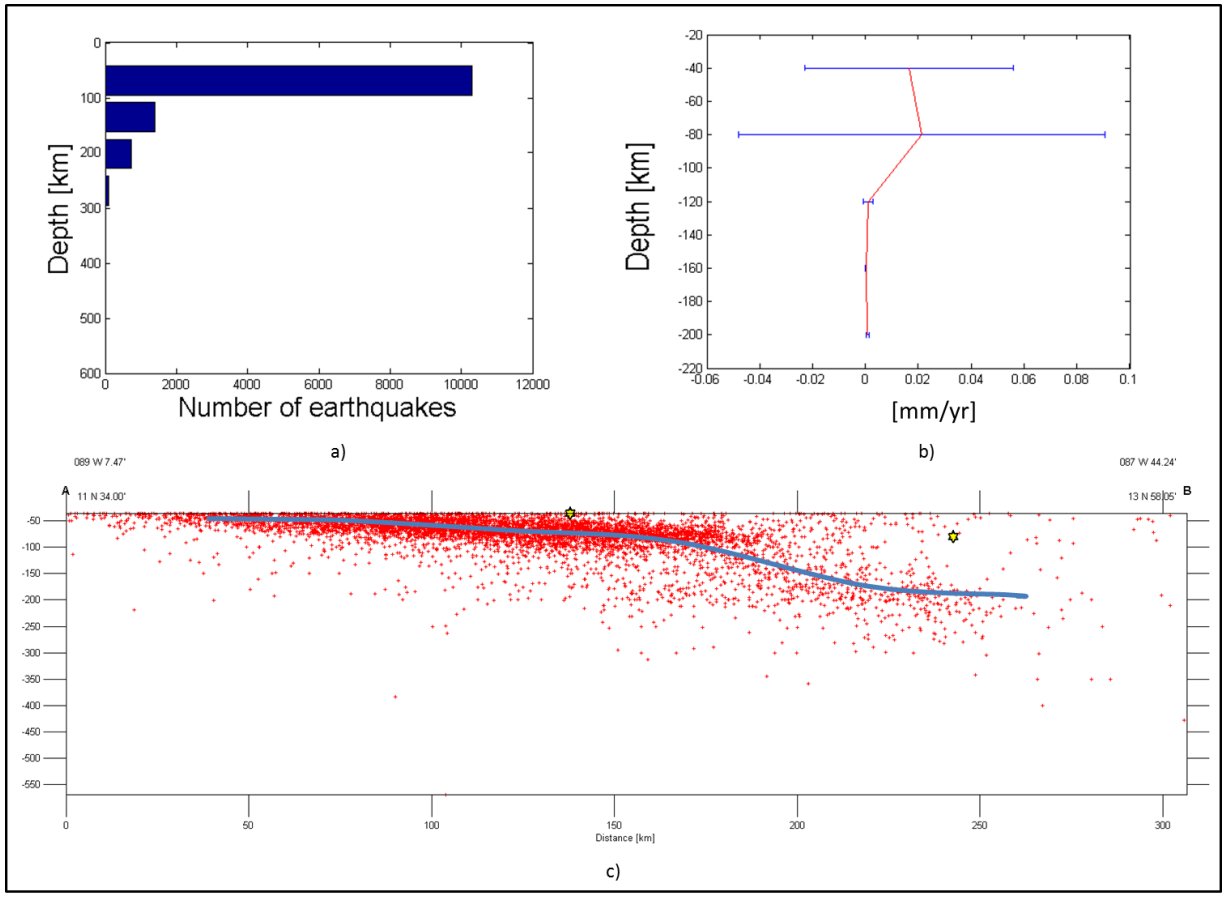

Figure 16. Block No. 2 a) Histogram of events, b) Horizontal Velocity of STD, c) Cross section of seismicity.

Block 3

This block is located at south broadside of Cuba and includes extension of Jamaica Island (Figures 14 and 17). Though is a low seismic activity zone, its major activity matches with the highest STD interval (Figure 17b). Figure 17c shows the direction of horizontal velocity of STD, oscillating between 30° and 60° for the unique depth range of deformation (35-40km).

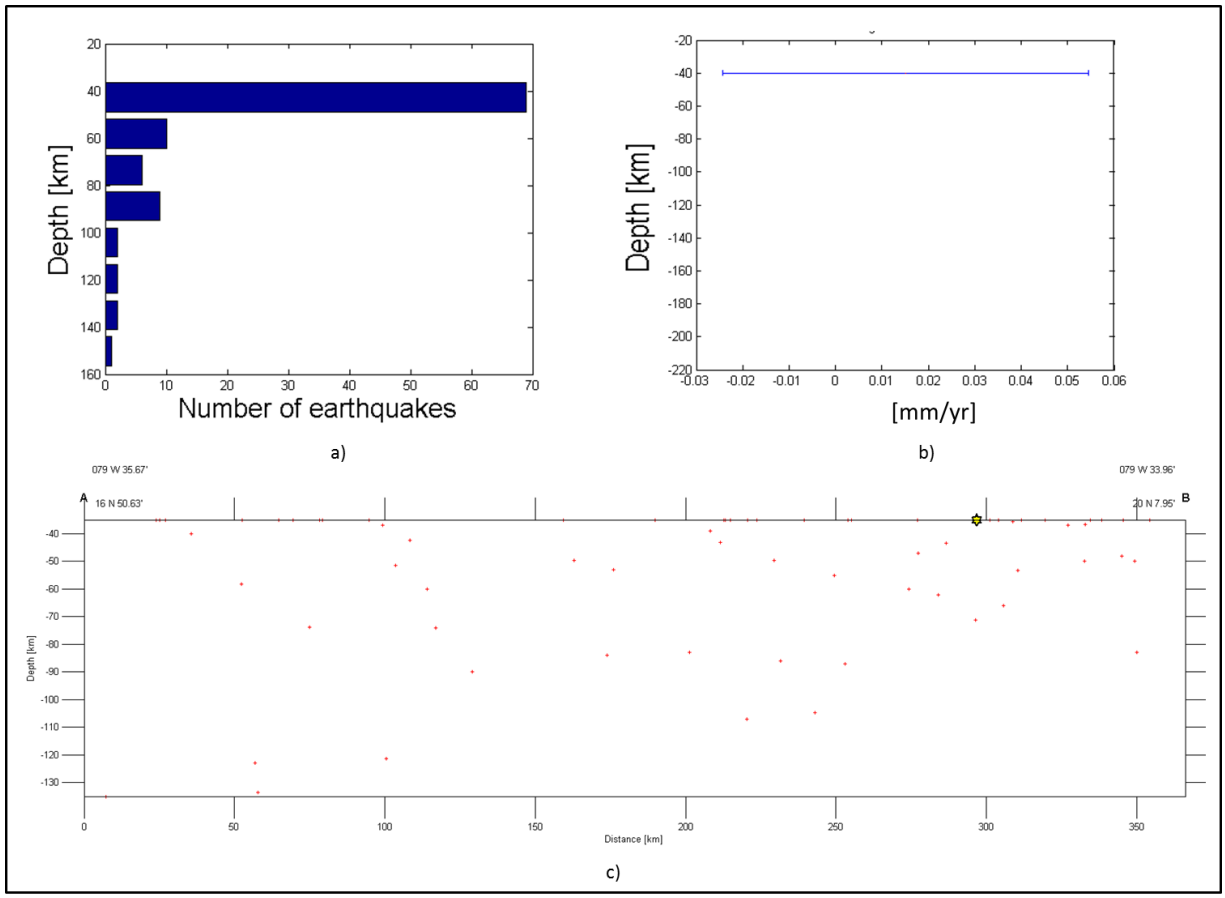

Figure 17. Block No. 3 a) Histogram of events, b) Horizontal Velocity of STD, c) Cross section of seismicity

Block 4

Encompasses the complex tectonic scenario of the Hispaniola Island, where is observed a flip of polarity and change of the subduction style (Figures 14 and 18).

Seismic activity is located mainly around the first 80km depth, with a relevant reduction up to 200km (Figure 18a). As in other intervals, same depth range of large activity matches with the highest STD values (Figure 18b). Tough is not conclusive, Figures18c suggests a domain of direction in horizontal velocity of STD toward the South broadside.

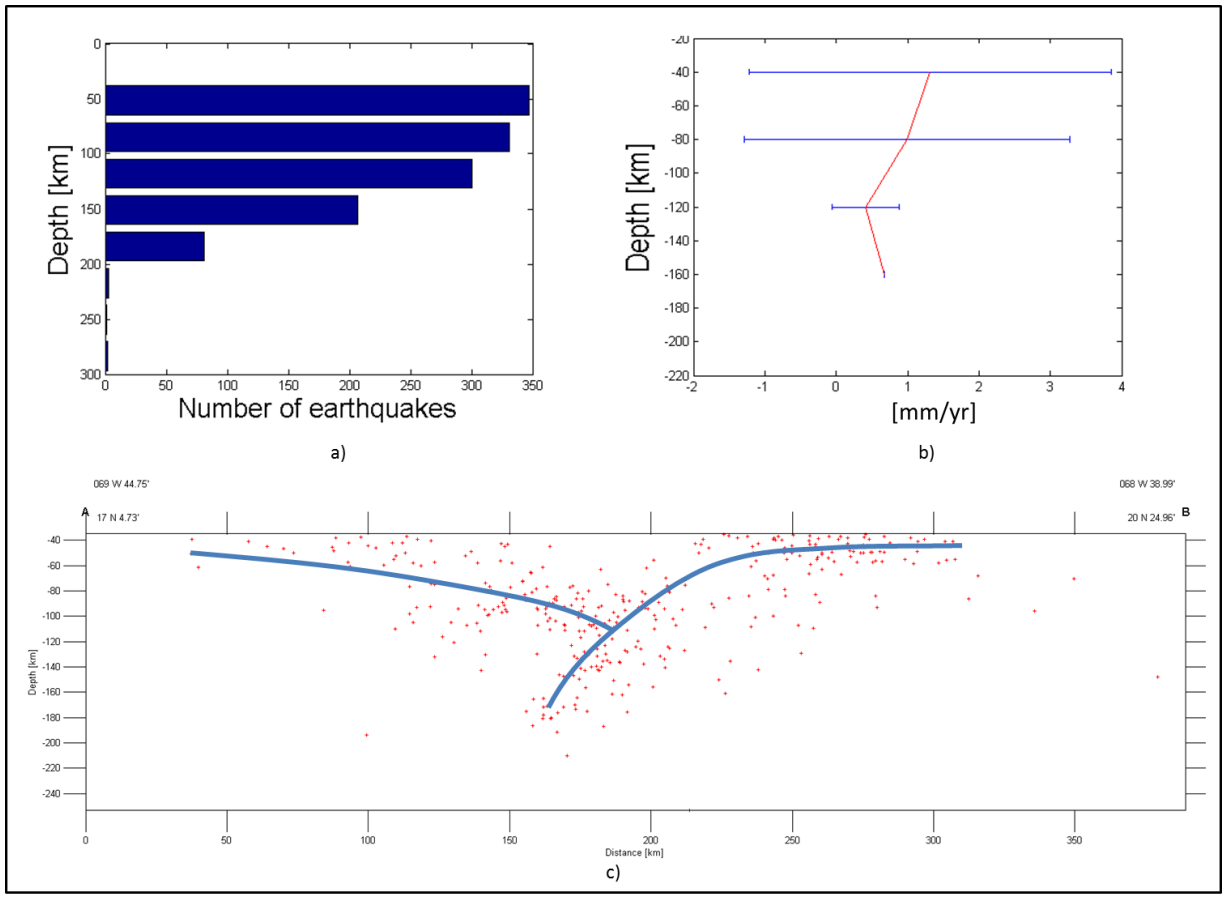

Figure 18. Block No. 4 a) Histogram of events, b) Horizontal Velocity of STD, c) Cross section of seismicity

Block 5

Located on intersection zone between Greater and Lesser Antilles (see Figures14 and 19), it shows the main seismic activity and sesimotectonic deformation in the range of 35 to 50km depth, with decreasing of these parameters in deeper intervals. Figure 19c indicates a trend of deformation in horizontal velocity of STD for the ranges between 0 and 80km with directions 300° to 330° and in the range 90°-120° in the interval 80 and 120km.

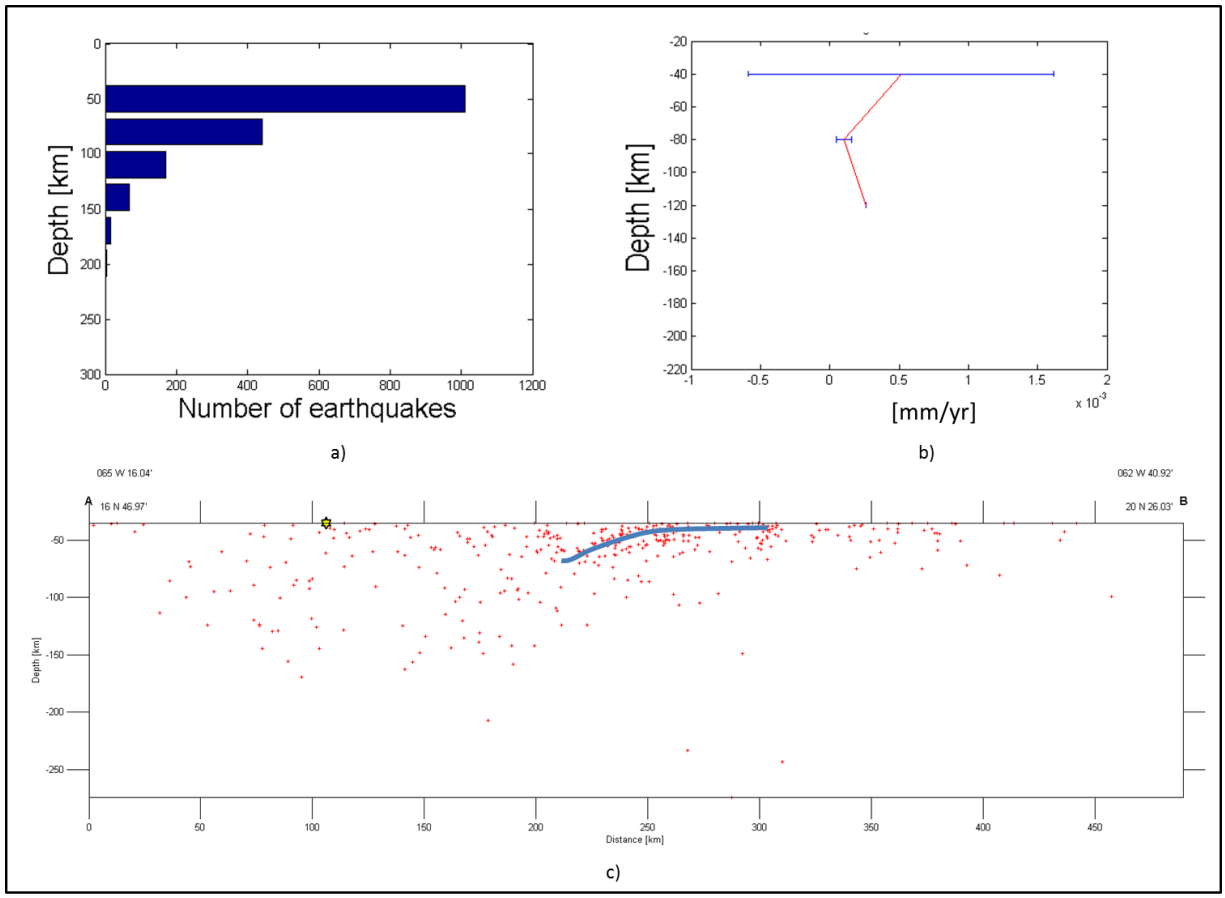

Figure 19. Block No. 5 a) Histogram of events, b) Horizontal Velocity of STD, c) Cross section of seismicity

Block 6

Located on Northern broadside of LA, covers the upper to mid intervals of the subduction structure (Figures 14 and 20). In this block was not found a correspondence in depth of the main seismic activity interval (35 – 50km) and the respective major STD interval, found in interval 120km to 160km (Figure 20a and 20b); neither a clear pattern of the STD direction (Figure 20c).

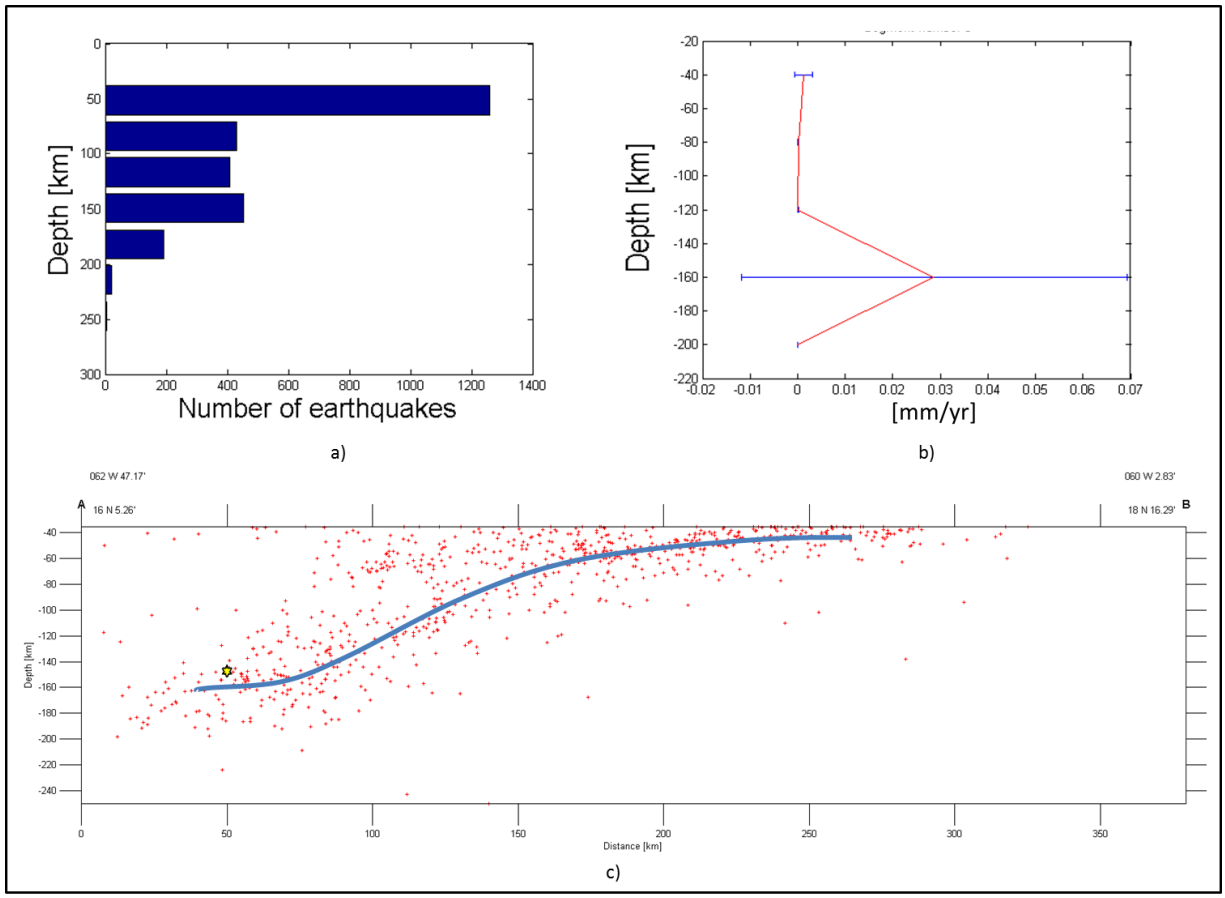

Figure 20. Block No. 6 a) Histogram of events, b) Horizontal Velocity of STD, c) Cross section of seismicity

Block 7

This region is located in southern section of subduction structure in LA. Histogram of the Figure 21a shows major seismic activity in the range 35km – 50km of depth, which is decreasing with depth; this situation is not totally represented through the horizontal velocity of STD (Figure 21b) which registers the main deformation in the firsts 80km depth. Figure 21c does not show a manifest trend of the deformation direction.

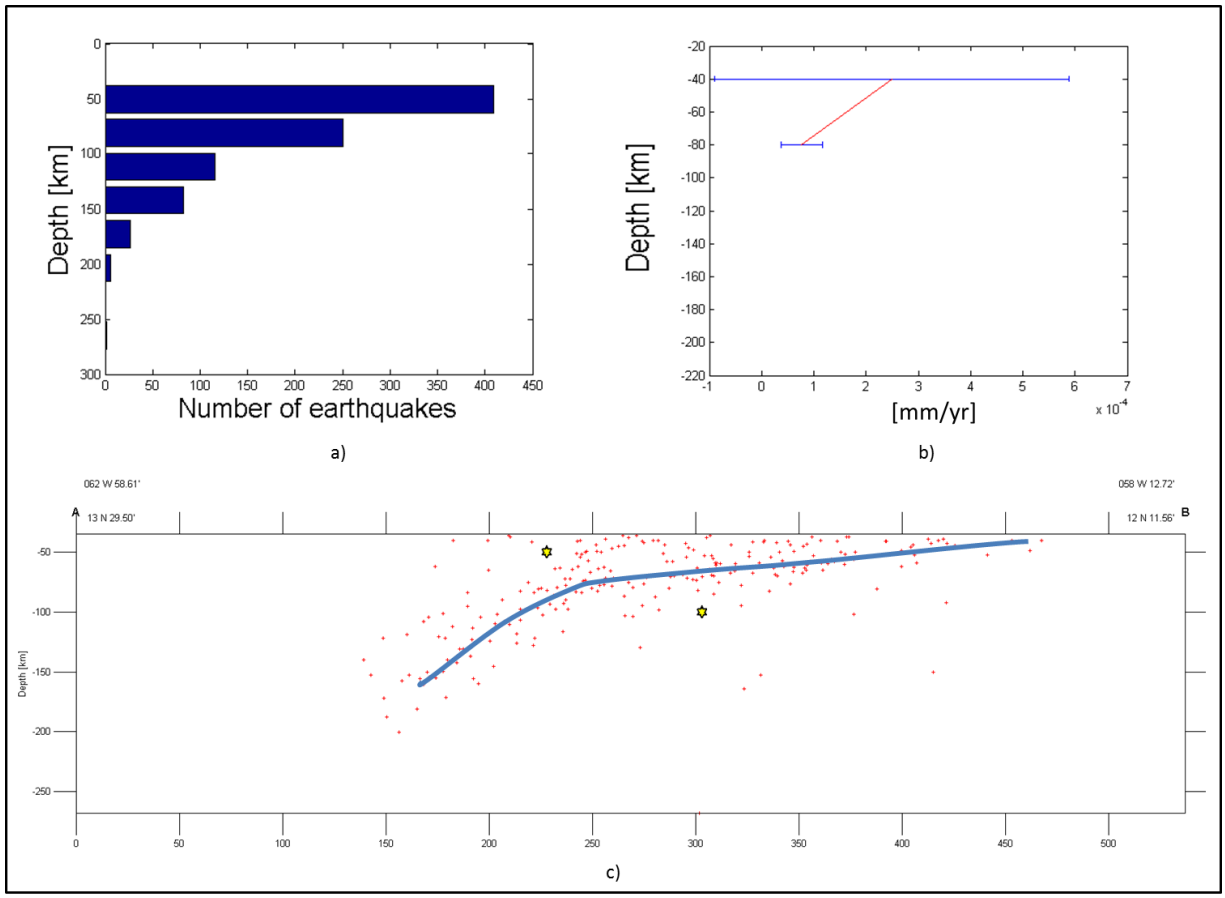

Figure 21. Block No. 7 a) Histogram of events, b) Horizontal Velocity of STD, c) Cross section of seismicity

Block 8

Block 8 is located at North of South American continent and southern of CAP (Figures 14 and 22). Seismic activity is located mainly in the interval 35 – 40km of depth (Figure 22a), where is registered the highest rate of STD too (Figure 22b). Figure 22c shows a variable direction of horizontal movement in relation with different depth ranges analyzed.

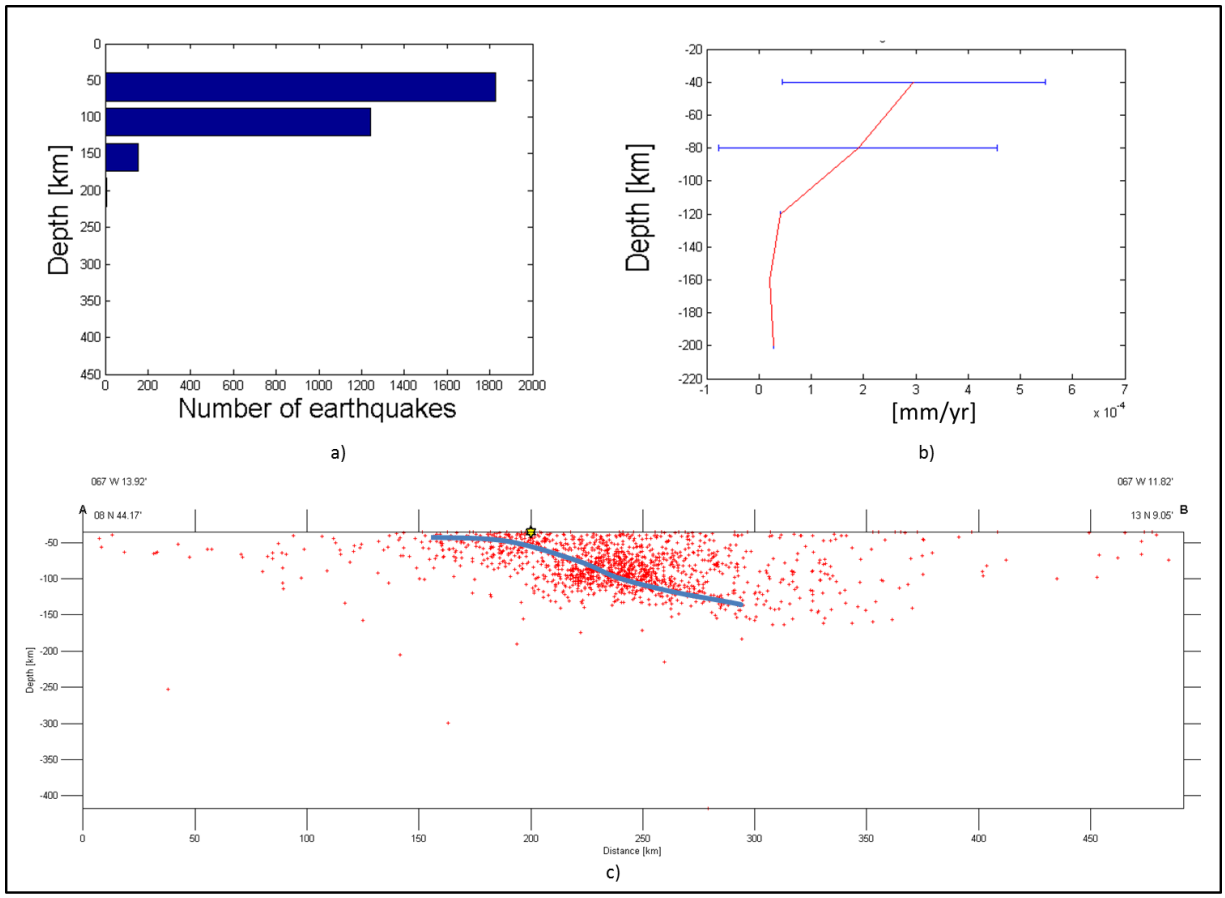

Figure 22. Block No. 8 a) Histogram of events, b) Horizontal Velocity of STD, c) Cross section of seismicity

Block 9

Block 9 is framed by Venezuela borderland, Bocono Fault and Bucaramanga-Santa Marta Fault at Northern of South American continent.

Graphics of characterization (Figure 23) show a correspondence of depth with seismic activity in interval from 35 to 200km of depth (Figure 23a), where is registered values of STD IN Figure 23b, however magnitudes are inverse due to number of events increasing with depth, while major horizontal velocity of STD is registered at shallowest depth (0-40km) and decreasing to 200 km too. Figure 23c shows a trend of directions of STD between 0 to 120km in 150°-210° and variables values for two last ranges of depth.

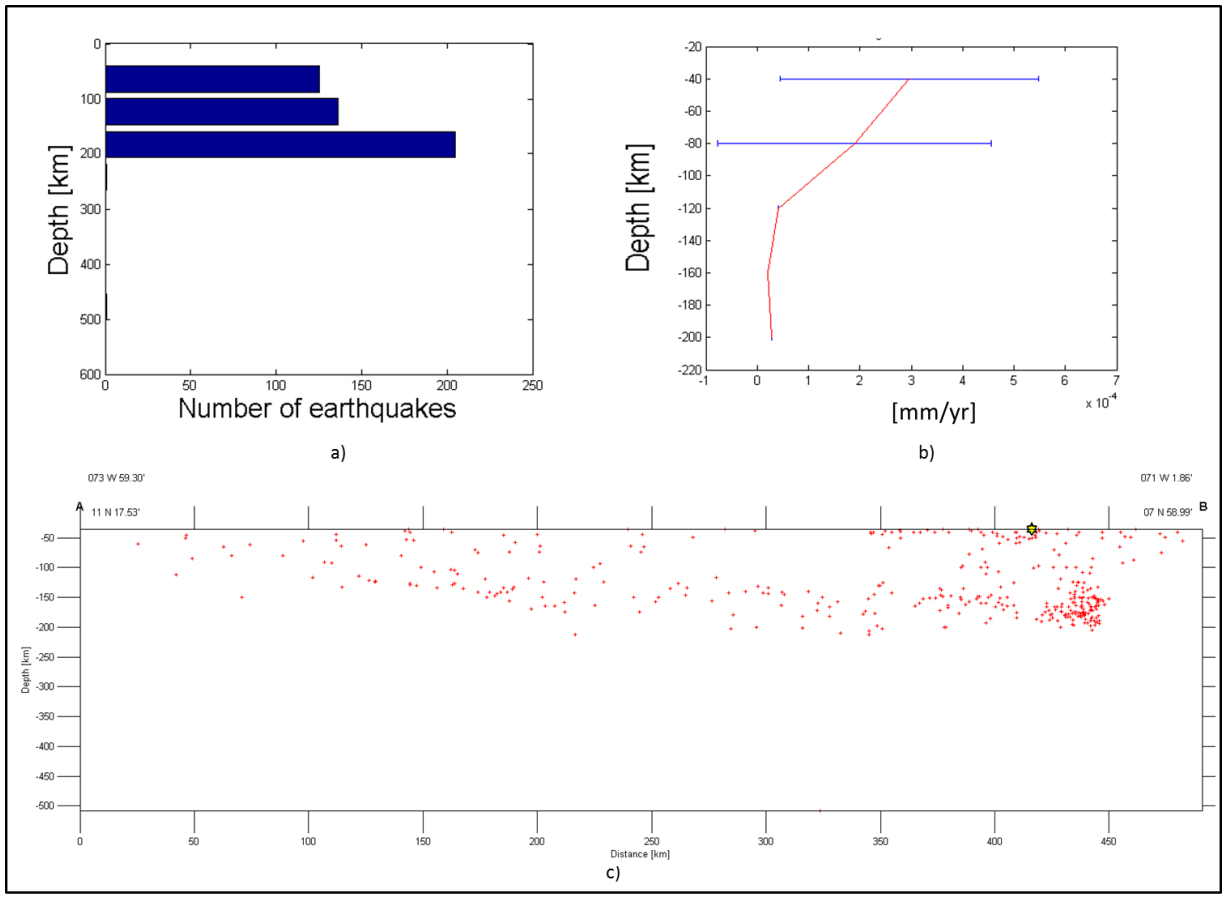

Figure 23. Block No. 9 a) Histogram of events, b) Horizontal Velocity of STD, c) Cross section of seismicity

Block 10

Block 10 involve structure located at Northern and Central zone of Colombia from boundary between CAP and SA plate to beginning of volcanic belt toward South zone is framed by Venezuela borderland, Bocono Fault and Bucaramanga-Santa Marta Fault at Northern of South American continent.

Graphics of characterization (Figure 24) show seismic activity before 80km, where is found a correspondence between plot of number of events (Figure 24a) and velocity of STD (Figure 24b), in the same way happen after 120km where low seismic activity is in concordance with slow STD. However, direction of STD is so variable for first 2 ranges where there is seismic activity while it is possible to see a trend between 0° to 30° for range depth from 120km to 200km.

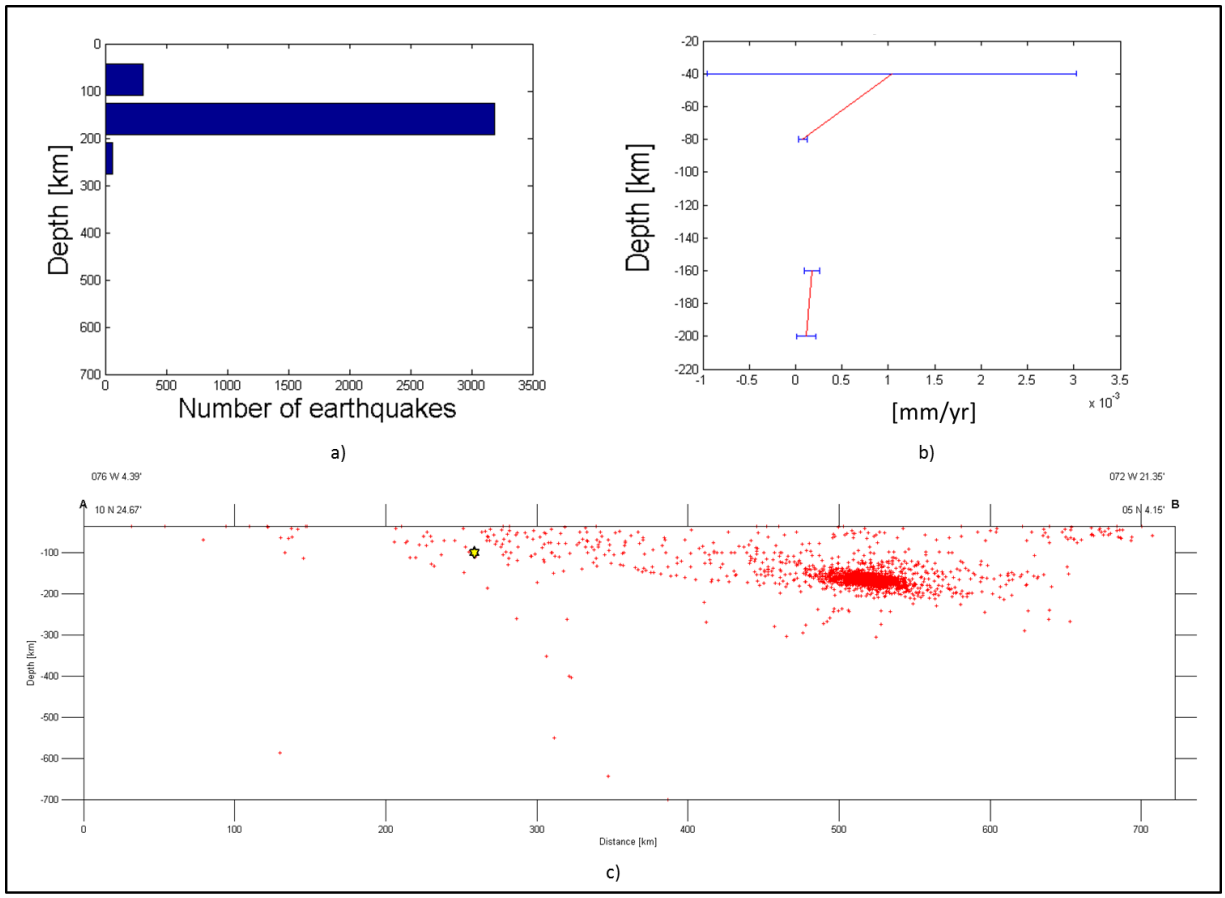

Figure 24. Block No. 10 a) Histogram of events, b) Horizontal Velocity of STD, c) Cross section of seismicity

Block 11

Block 11 is located in section eastern of Panama country report shallow seismic activity exactly in gap zone where there are not evidence of active volcanism.

Figure 25 show slow seismic activity with low number of events (Figure 25a) between 35 to 80km and little velocity of STD values (Figure 25b) which contrast directly with segments delimited at eastern and western side. Furthermore, it is evident a trend in orientation of velocity of STD in range between 30° and 60° (Figure 25c).

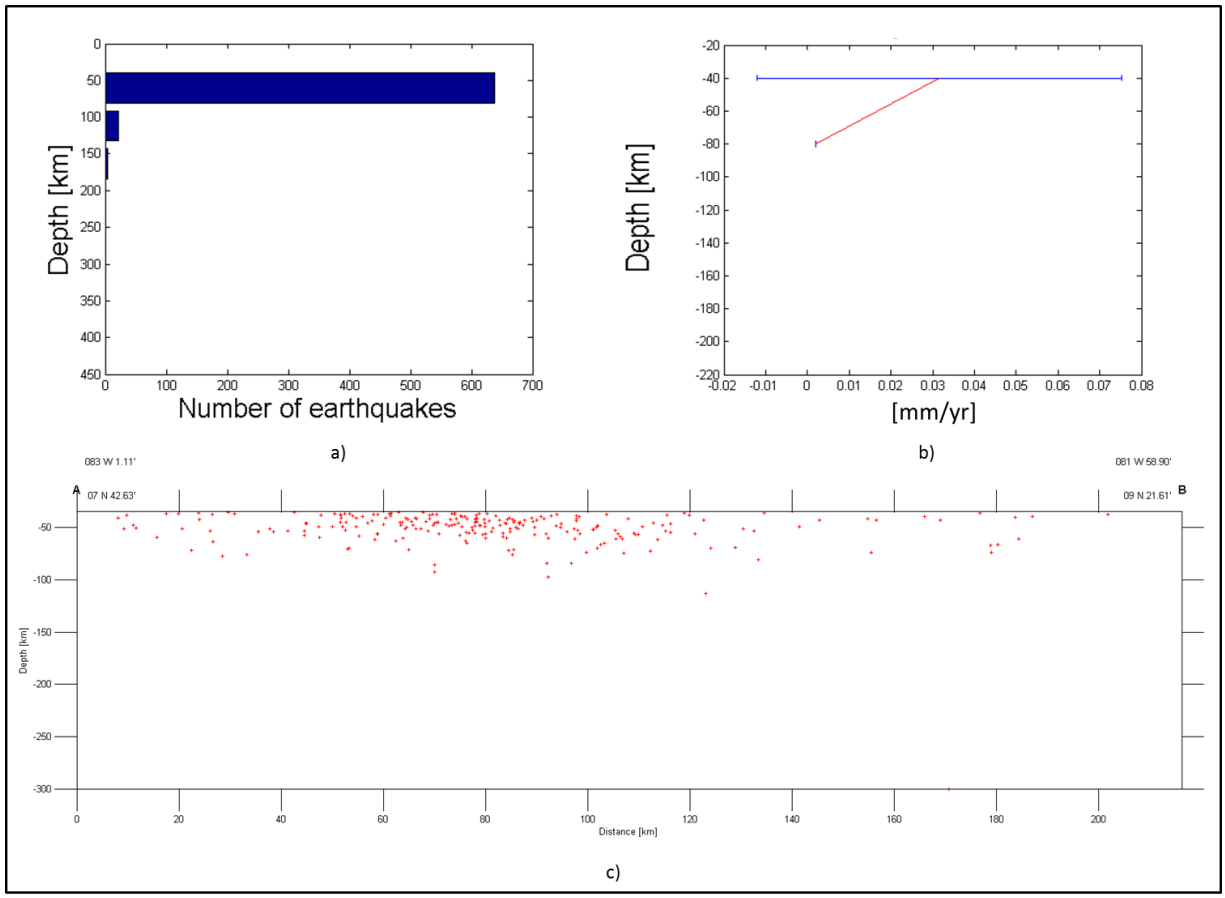

Figure 25. Block No. 11 a) Histogram of events, b) Horizontal Velocity of STD, c) Cross section of seismicity

Block 12

Block 12 is located in a zone that cover Panama arc, Pacific coast of Colombia where is extended into continent to eastern boundary of Central Belt.

Figure 26a reveals a clear increment of number of events registered in shallower ranges of analysis. So, seismic activity decreasing after 80km to 300km while a different situation is evidenced from plot of STD (Figure 26b) where there are more homogeneity in rates of STD between 0 and 200km. Moreover, (Figure 26c) indicate high variability and it is not clear to speak about possible trend in direction of movement.

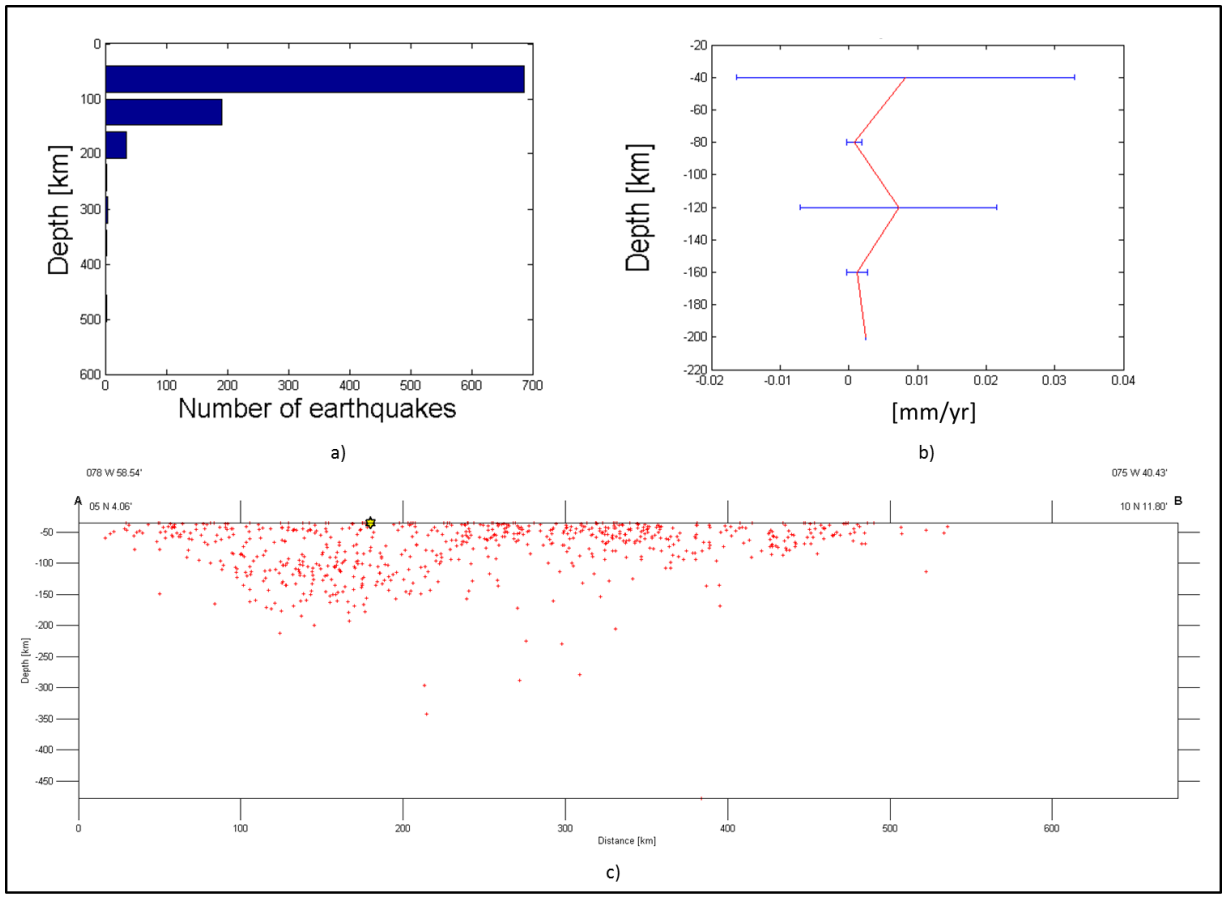

Figure 26. Block No. 12 a) Histogram of events, b) Horizontal Velocity of STD, c) Cross section of seismicity

Block 13

Block 13 corresponds to gap of volcanic mountain on AM in Colombia with front in the Cocos Ridge and MAT. Histogram of frequency of seismicity for the zone (Figure 27a) shows seismicity level with a low number of events concentered from 80 to 120km mainly. This situation responds to little values gotten in plot of velocity of STD (Figure 27b) without trend in angle of direction of STD (Figure 27c).

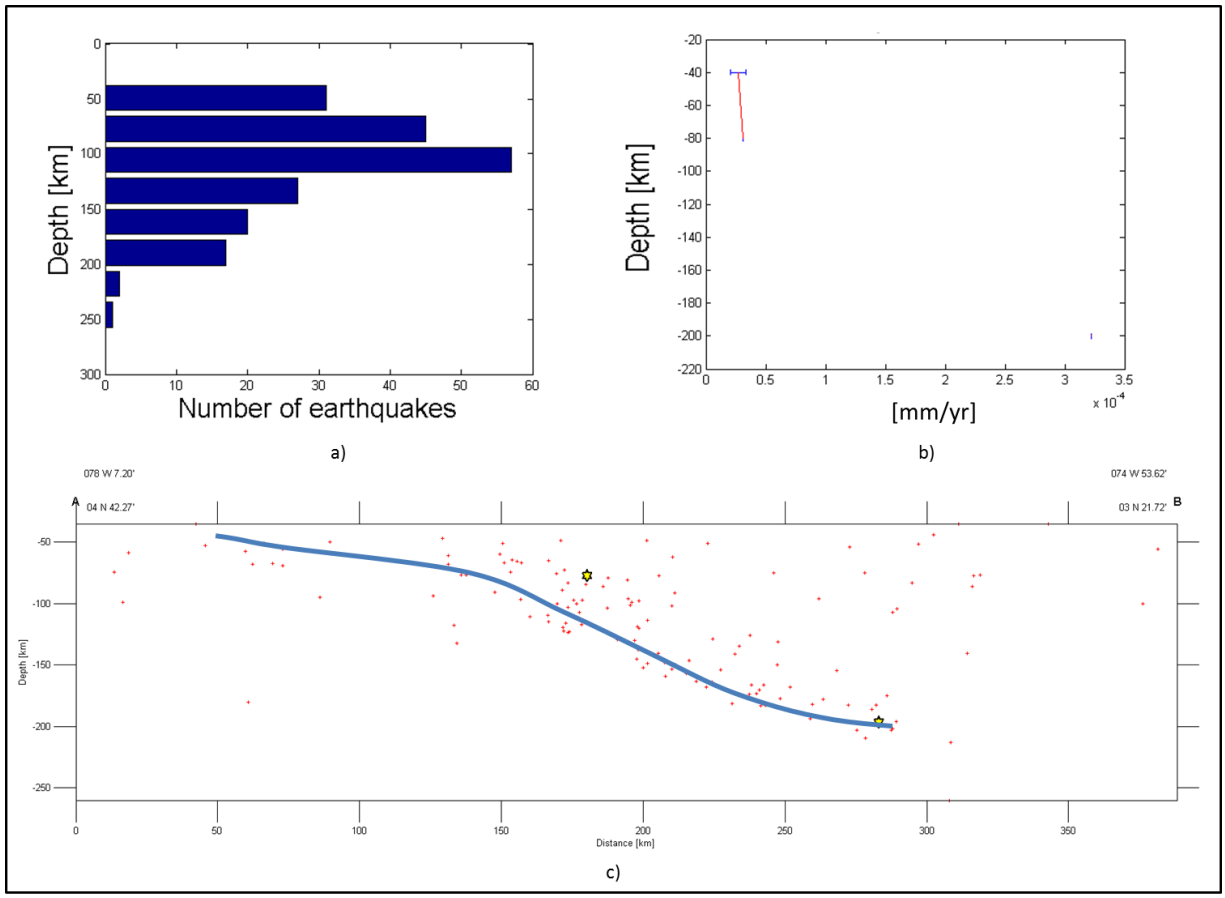

Figure 27. Block No. 13 a) Histogram of events, b) Horizontal Velocity of STD, c) Cross section of seismicity

Block 14

Block 14 involves Southeastern side in Colombia, where is located active volcanic line in Colombia and boundary with Ecuador.

Graphics of characterization displayed in Figure 28 note the main deformation in first 80 km of depth (Figure 28a), situation is conserved in plot of STD (Figure 28b), which do not happened with Rose diagrams (Figure 28c) where is not represented a clear trend of movement.

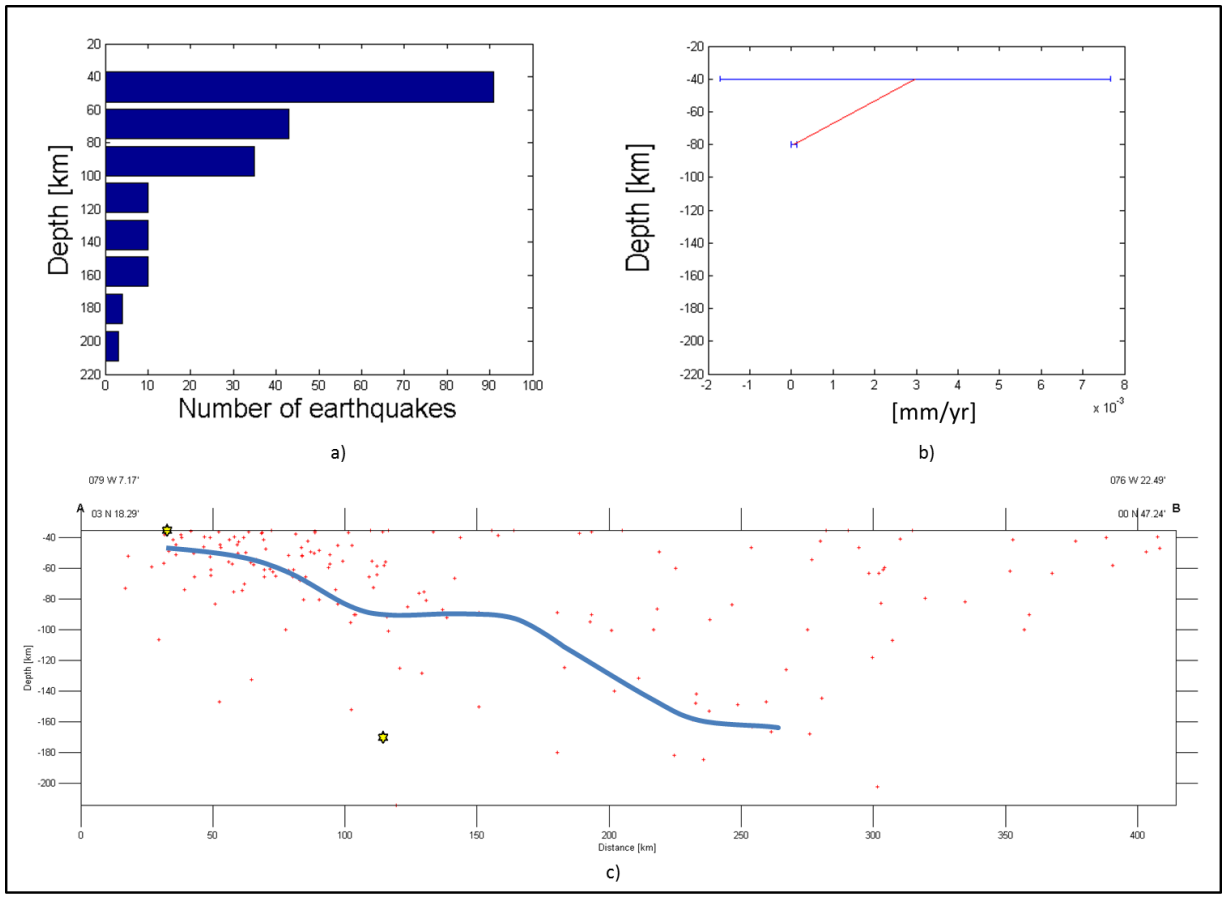

Figure 28. Block No. 14 a) Histogram of events, b) Horizontal Velocity of STD, c) Cross section of seismicity

Block 15

Block 15 involves an extension covered by Ecuador country, zone which is influenced by tectonic activity of Cambridge Ridge and coarsening of volcanic lines.

Graphics of characterization displayed in Figure 29, the main deformation is presented by the first 80km (Figure 29a), which correspond with Figure 29b but does not report a trend of movement direction (Figure 29c).

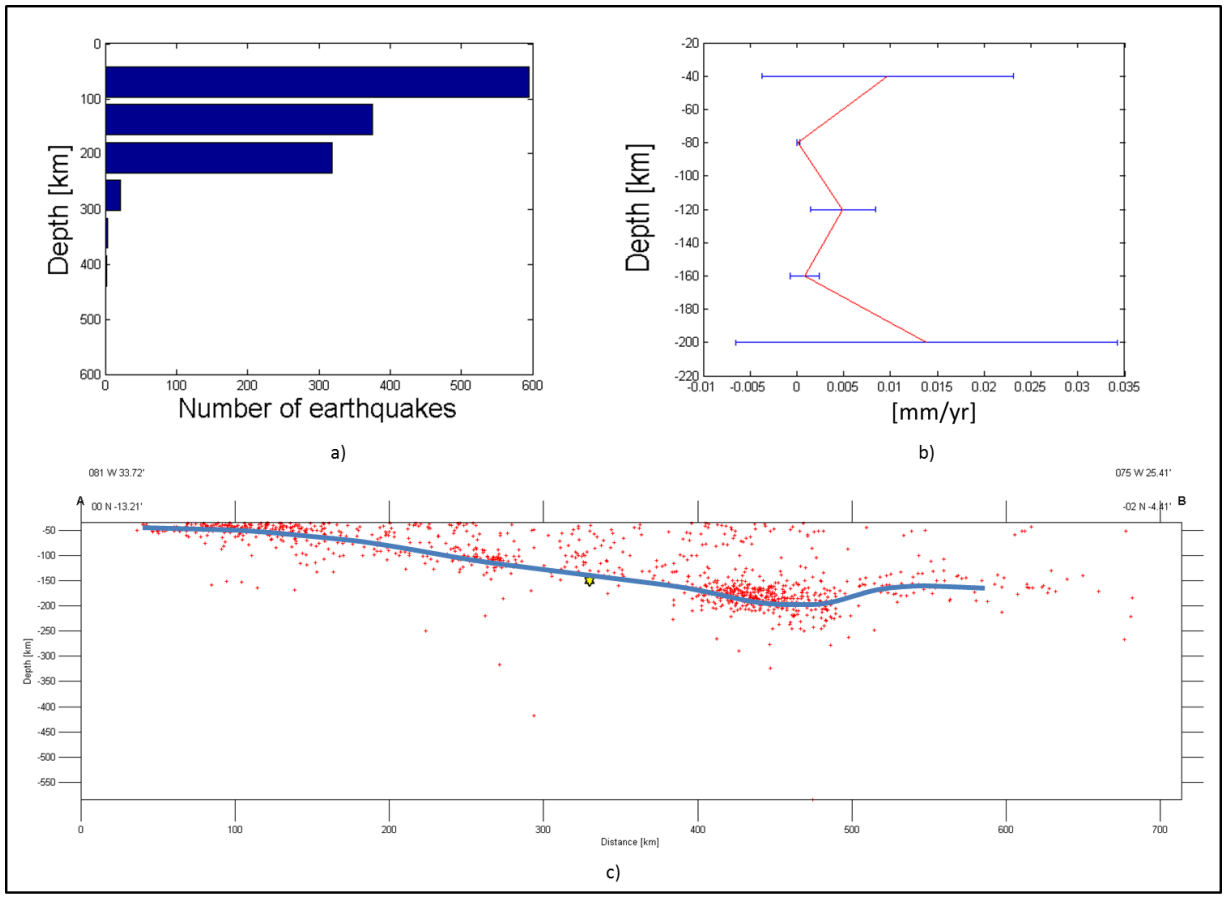

Figure 29. Block No. 15 a) Histogram of events, b) Horizontal Velocity of STD, c) Cross section of seismicity

Block 16

Block 16 is extended from end of volcanic mountain in Ecuador, near to boundary between Ecuador and Peru to finishing of gap along to PCT in point where is presented an influence of NZR.

Plots of characterization displayed in Figure 30a respond to major seismic activity before first 100km of depth and decreasing to 680km, this situation is represented too through graphic of STD for the first 200km. Analyzing rose diagrams (Figure 30c) it was found that there are not a trend defined in angle of direction of STD.

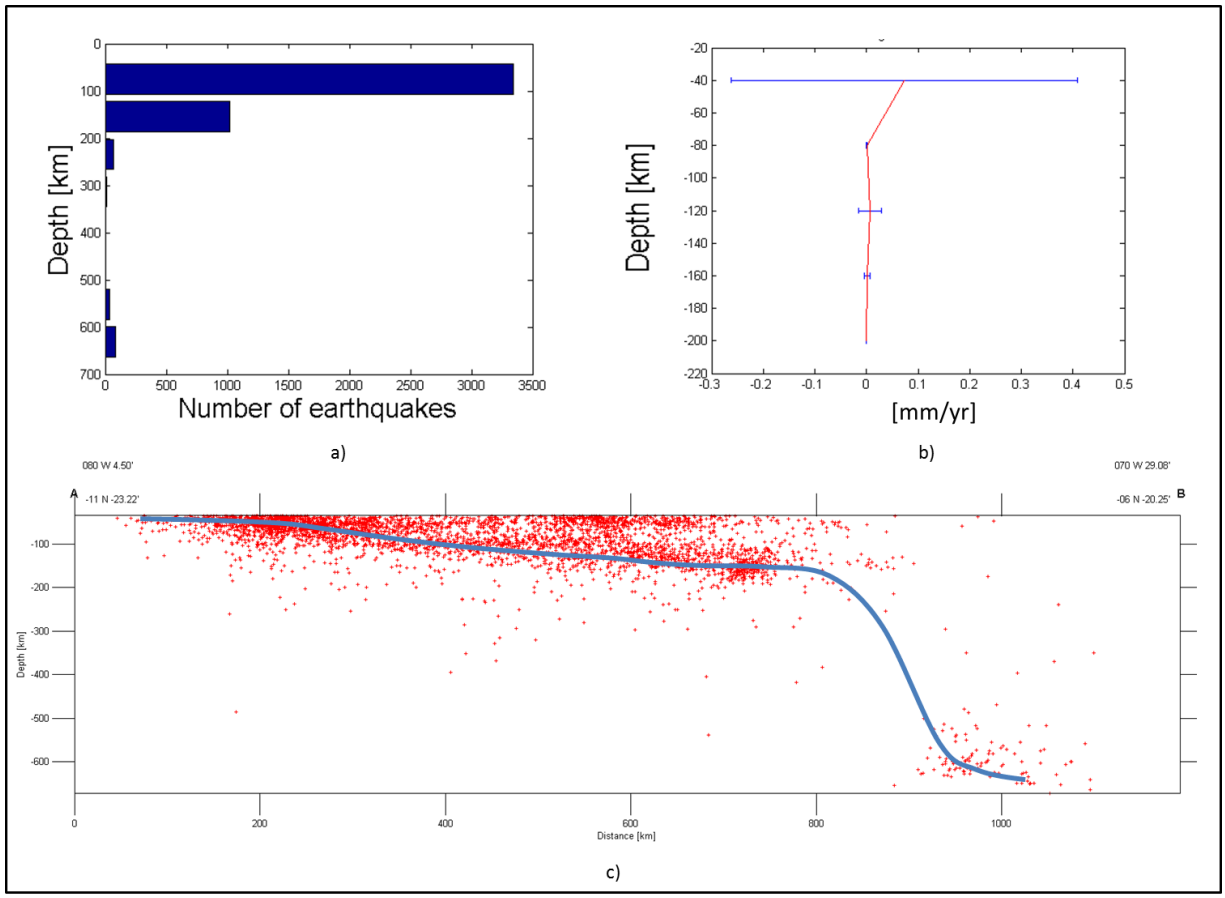

Figure 30. Block No. 16 a) Histogram of events, b) Horizontal Velocity of STD, c) Cross section of seismicity

Block 17

Block 17 is extended from beginning of volcanic line in sense north-south to point where is presented a change in distribution of volcanoes and therefore a change of type of subduction.

For this zone, have been registered earthquakes to 700 km of depth, with special concentration on first 350km, where values with velocity of STD (Figure 31b) are near to described in Figure 31a. In addition, Figure 31c shows a trend after 40km with an angle of direction of STD between 60° and 90°.

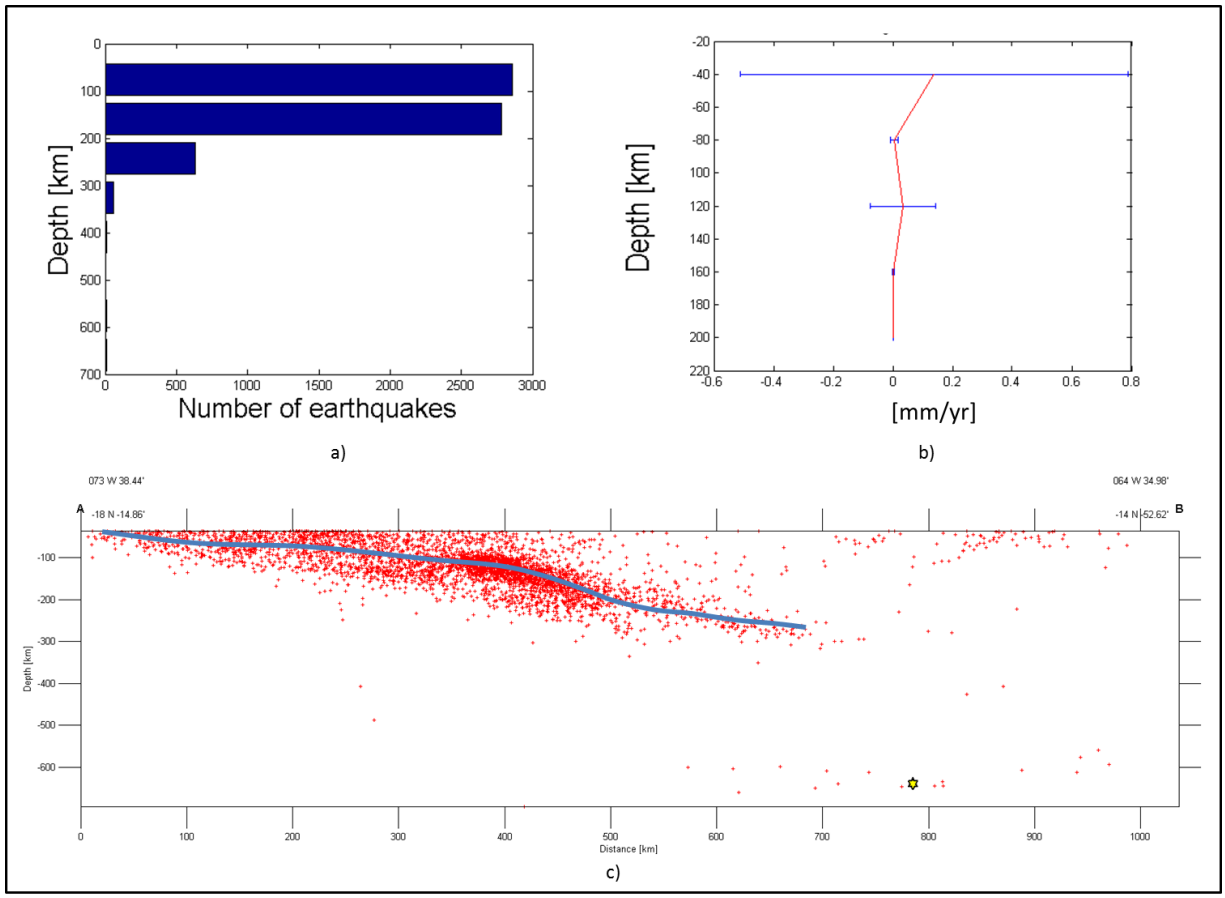

Figure 31. Block No. 17 a) Histogram of events, b) Horizontal Velocity of STD, c) Cross section of seismicity

Block 18

Segment 18 is delimited between latitudes 20°Sto 28°Son line of 68°W of longitude and covers volcanic structure in Chile.

Seismotectonic parameters indicate a notable increasing in seismic activity before 200km of depth (Figure 32a), range where is presented little rates of seismotectonic deformation from solutions of focal mechanism (Figure 32b). In the other hand is not possible define a clear trend of velocity of STD , however range between 60° and 90° is the most frequent throughout different ranges of depth.

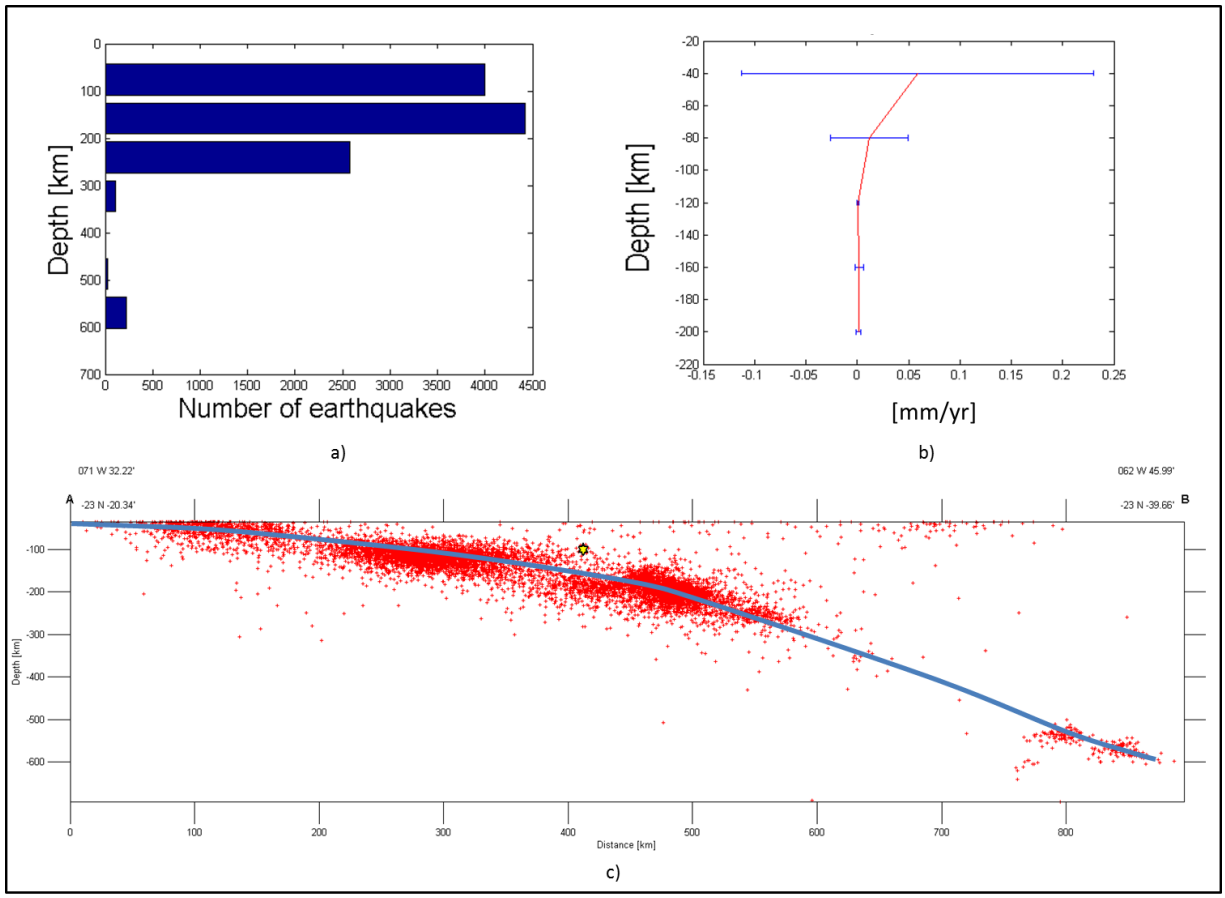

Figure 32. Block No. 18 a) Histogram of events, b) Horizontal Velocity of STD, c) Cross section of seismicity

Block 19

Block 19 extends from limit of above segment to latitude around 35°S along to convergence margin of PCT.

So, graphics of Figure 33 indicates a correspondence between range with major number of earthquakes recorded by catalogue and rates of horizontal STD which beginning near to 1.0 mm/yr and decreasing near to 0 to 200km of depth. Rose diagrams (Figure 33c) do not report trend in direction of velocity of movement in horizontal component.

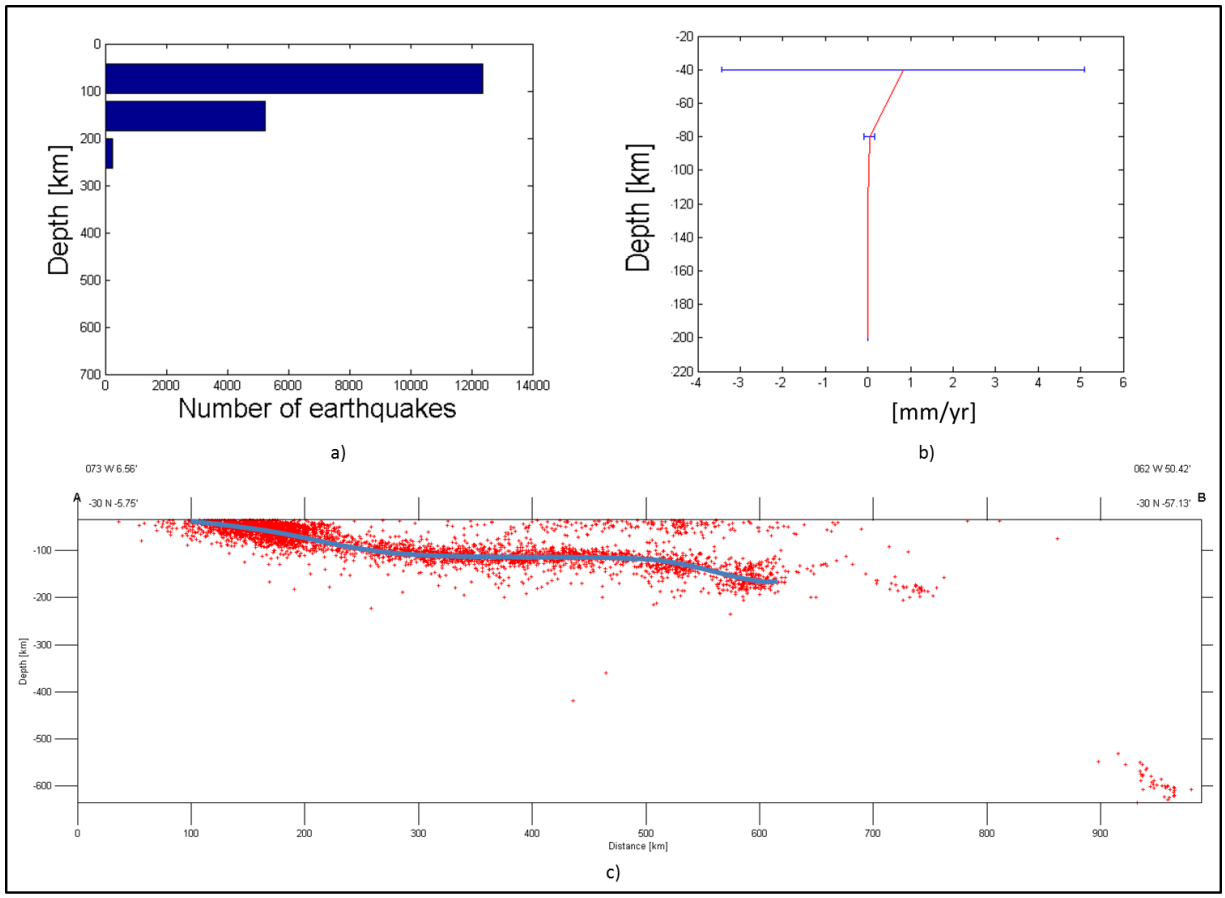

Figure 33. Block No. 19 a) Histogram of events, b) Horizontal Velocity of STD, c) Cross section of seismicity

Block 20

Block 20 is extended from 35°S to end of Southern segment of Volcano Mountains in Chile associated to PCT as margin of convergence among tectonic plates.

Graphics of seismotectonic characterization (Figure 34) responds to situation and represent high seismicity at the first meters of depth with a next decreasing to range near to 200km. For this case, trend present difficult for establishing but angle with more domain is between 30° and 60° mainly for the last 120km of analysis (80km - 200km).

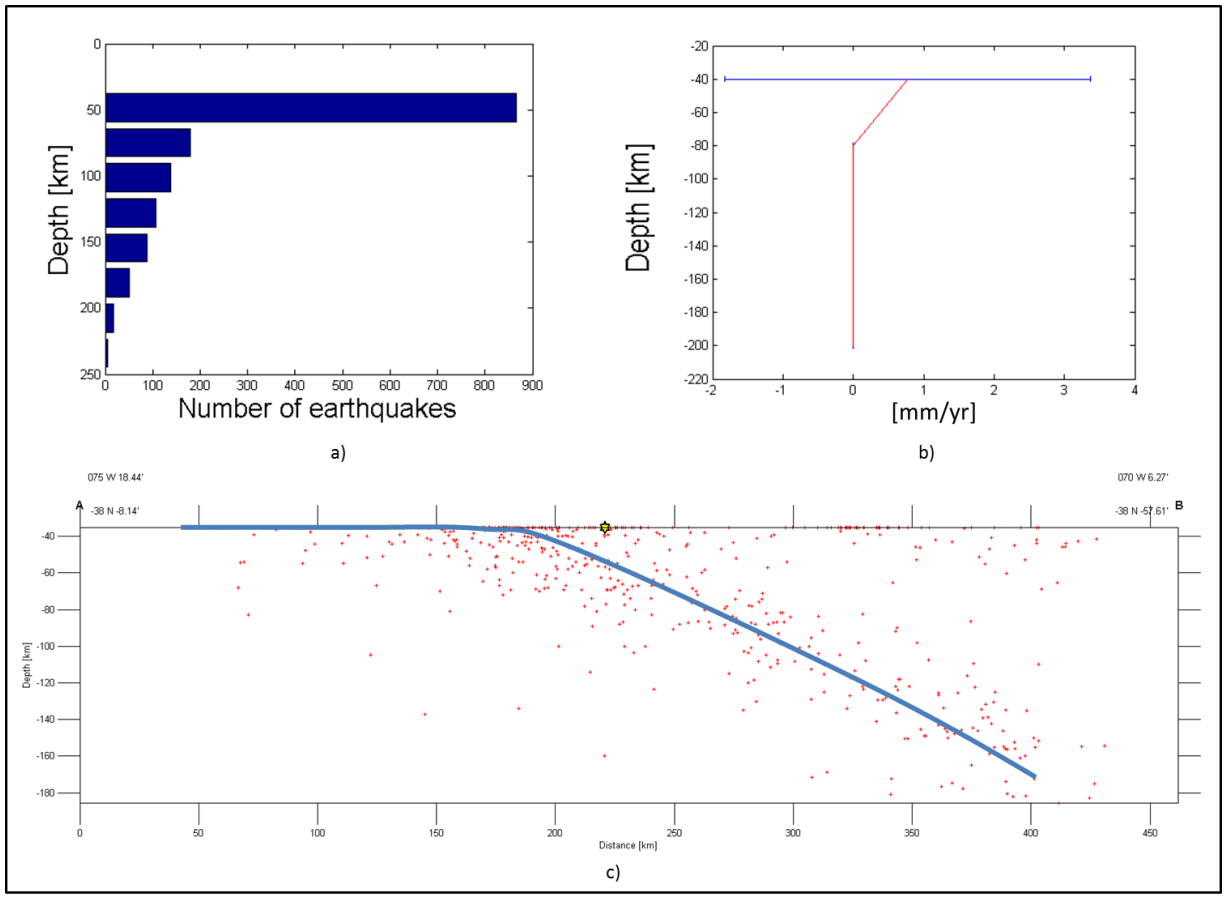

Figure 34. Block No. 20 a) Histogram of events, b) Horizontal Velocity of STD, c) Cross section of seismicity

Block 21

Finally, Block 21 is extended a long a called Patagonian Andes with front in an incipient subduction zone marked by SFZ.

Based on the above, plots displayed in Figure 35 show a deformation for this segment which is located only for shallow depth, with a maximum equal to 60km of depth and an orientation of the horizontal velocity of STD between 210° and 240°.

From above graphics, Table 4 presents a summary with main characteristics geotectonic for each proposal block in order to know seismic potential as contribution to understanding of subduction regions into source parameters for hazard model.

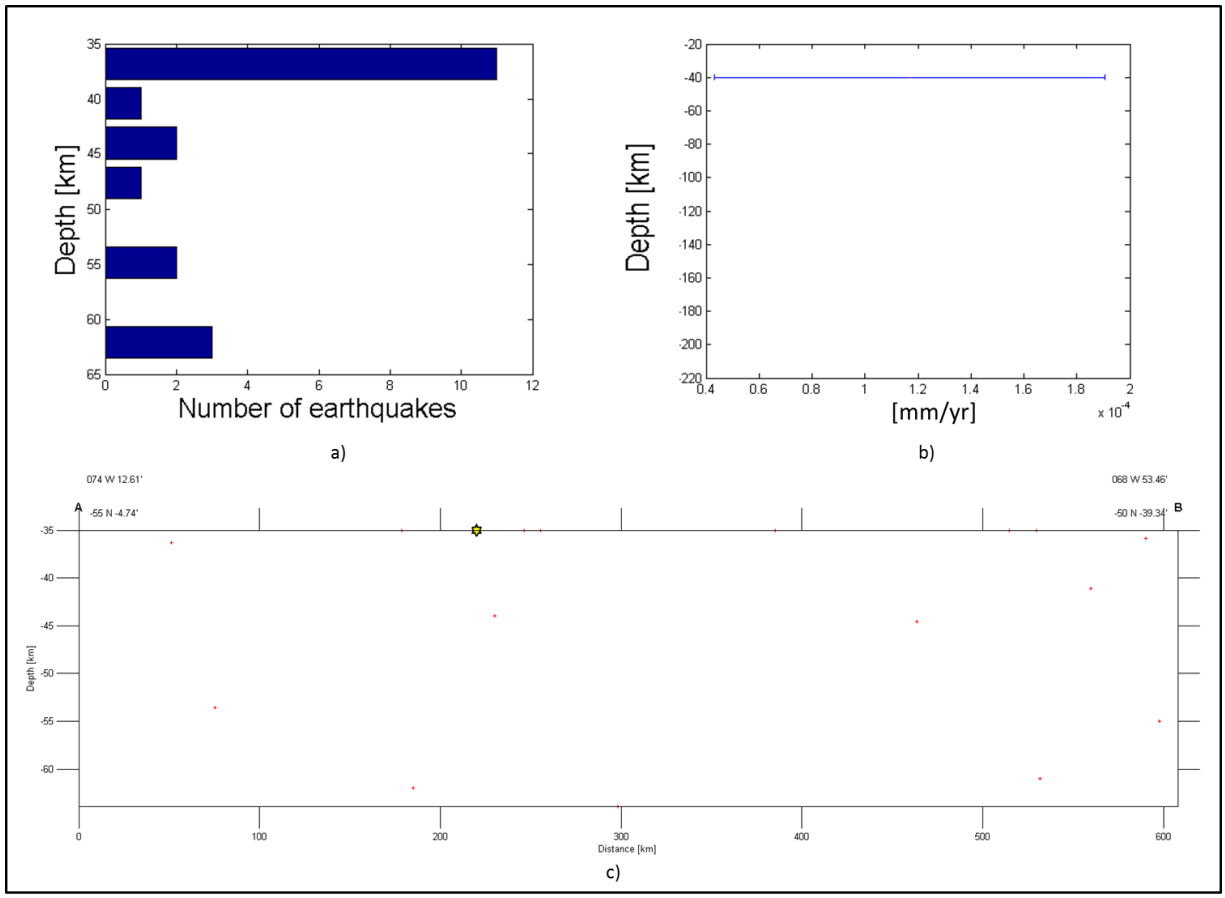

Figure 35. Block No. 21 a) Histogram of events, b) Horizontal Velocity of STD, c) Cross section of seismicity

Table 4. Summary of Seismotectonic Blocks along subduction zones in South American western boundary

Block	Area [km2]	FMD Parameters			Slab Dip			Seismotectonic Deformation			
		b value ±	a value	Mc	InitialAngle [Deg]	Max. Angle [Deg]	Distance of Max. Angle [km]	Depth [km]	Horizontal Velocity of STD	Standard Desviation	Direction Rumbo
1	499543,0342	0,80125±0,063	6,02	4,8	14,7	15,1	370	0-40	0,089611	0,207751	60°-90°
								40-80	0,014304	0,044889	30°-60°
								80-120	0,002308	0,004586	30°-60°
								120-160	0,001389	0,002260	60°-90°
								160-200	0,007929	0,012224	30°-60°
2	406590,6007	1,0485±0,13	7,225	5	20,6	29,0	220	0-40	0,016393	0,039372	30°-60°
								40-80	0,021201	0,069229	30°-60°
								80-120	0,000905	0,001778	30°-60°
								120-160	0,000127	0,000077	30°-60°
								160-200	0,000770	0,000631	30°-60°
3	283643,8084	0,749±0,1	5,24	4,9	-	-	-	0-40	0,015139	0,039456	0°-330°
								40-80	NaN	NaN	NaN
								80-120	NaN	NaN	NaN
								120-160	NaN	NaN	NaN
								160-200	NaN	NaN	NaN
4	225283,0395	1,17±0,1	7,91	4,9	45,0	52,4	50	0-40	0,001317	0,002540	300°-330°
								40-80	0,000995	0,002281	270°-300°
								80-120	0,000413	0,000475	90°-300°
								120-160	0,000676	0,000000	240-270°
								160-200	NaN	NaN	NaN
5	186459,2479	1,81±0,2	11,1	4,9	9,5	14,0	100	0-40	0,000514	0,001101	300°-330°
								40-80	0,000102	0,000055	300°-360°

								80-120	0,000258	0,000000	90°-120°
								120-160	NaN	NaN	NaN
								160-200	NaN	NaN	NaN
6	184063,3937	1,34±0,09	8,97	4,8	11,3	42,6	125	0-40	0,001215	0,001881	270°-360°
								40-80	0,000150	0,000141	330°-360°
								80-120	0,000094	0,000117	0°-60°, 210°-240°
								120-160	0,028726	0,040604	30°-60°, 300°-330°
								160-200	0,000014	0,000000	240°-270°
7	227179,3052	1,49±0,2	9,27	4,8	9,5	41,6	290	0-40	0,000249	0,000339	330°-120°, 270°-300°
								40-80	0,000077	0,000039	30°-60°, 330°-360°
								80-120	NaN	NaN	NaN
								120-160	NaN	NaN	NaN
								160-200	NaN	NaN	NaN
8	429715,2241	1,41±0,1	9,19	4,9	38,7	40,6	105	0-40	0,002432	0,004394	60°-90°, 150°-210°, 240°-300°
								40-80	0,001062	0,002021	60°-150°, 210°-270°, 330°-30°
								80-120	0,000165	0,000000	120°-150°
								120-160	0,000014	0,000020	90°-120°, 330°-360°
								160-200	NaN	NaN	NaN
9	194331,2453	1,56±0,2	9,55	4,9	-	-	-	0-40	0,000296	0,000252	
								40-80	0,000190	0,000267	150°-210°
								80-120	0,000041	0,000000	150°-180°
								120-160	0,000020	0,000000	180°-210°
								160-200	0,000029	0,000000	210°-240°
10	245730,8897	1,56±0,1	9,92	4,9	-	-	-	0-40	0,001037	0,001990	30°-60°

								40-80	0,000077	0,000046	180°-210°
								80-120	NaN	NaN	30°-60°, 150°-180°, 300°-360°
								120-160	0,000173	0,000084	0°-30°
								160-200	0,000116	0,000106	0°-30°, 210°-240°
11	63556,93593	0,606±0,1	4,57	5,1	-	-	-	0-40	0,031521	0,043650	0°-60°
								40-80	0,001961	0,000000	30°-60°
								80-120	NaN	NaN	NaN
								120-160	NaN	NaN	NaN
								160-200	NaN	NaN	NaN
12	369063,4164	1,14±0,2	7,53	4,9	-	-	-	0-40	0,008254	0,024613	0°-30°
								40-80	0,000825	0,001096	0°-30°
								80-120	0,007246	0,014311	240°-270°
								120-160	0,001214	0,001475	240°-270°
								160-200	0,002521	0,000000	0°-30°
13	46454,5806	1,03±0,1	6,47	4,7	26,6	36,9	190	0-40	0,000027	0,000006	60°-90°, 180°-210°
								40-80	0,000031	0,000000	330°-360°
								80-120	NaN	NaN	NaN
								120-160	NaN	NaN	NaN
								160-200	0,000322	0,000000	0°-60°
14	188294,2051	0,977±0,1	6,54	4,7	26,6	35,0	200	0-40	0,002967	0,004690	180°-210°, 330°-360°
								40-80	0,000068	0,000072	0°-30°, 90°-120°, 150°-210°
								80-120	NaN	NaN	NaN
								120-160	NaN	NaN	NaN
								160-200	NaN	NaN	NaN
15	323675,2663	0,8±0,05	6,1	4,7	19,3	20,6	400	0-40	0,009688	0,013458	150°-210°, 330°-

											360°
								40-80	0,000151	0,000196	180°-210°
								80-120	0,004919	0,003506	60°-90°
								120-160	0,000855	0,001559	60°-90°
								160-200	0,013817	0,020394	60°-90°
16	1487125,284	1,17±0,113	8,176666667	5	26,6	76,0	950	0-40	0,073189	0,336316	0°-30°
								40-80	0,000617	0,001266	180°-210°, 330°-360°
								80-120	0,006257	0,022216	270°-300°
								120-160	0,001534	0,005898	240°-270°
								160-200	0,000219	0,000223	60°-90°
17	667386,4199	1,17±0,05	8,6	4,9	16,7	42,0	500	0-40	0,137790	0,649619	0°-30°
								40-80	0,005412	0,012540	0°-30°
								80-120	0,033857	0,108835	60°-90°
								120-160	0,002208	0,002814	60°-90°
								160-200	0,001117	0,001014	60°-90°
18	886241,3626	1,03±0,03	8,08	4,8	21,8	28,8	800	0-40	0,058916	0,171685	0°-30°, 150°-180°
								40-80	0,011970	0,038015	60°-90°, 150°-180°, 210°-270°
								80-120	0,000536	0,000946	60°-90°
								120-160	0,002040	0,003820	60°-90°
								160-200	0,001342	0,002181	210°-240°
19	830155,5481	0,925±0,04	7,095	4,7	19,3	21,8	500	0-40	0,832059	4,265847	0°-30°, 150°-180°
								40-80	0,035513	0,121203	330°-60°
								80-120	0,000440	0,000760	240°-270°
								120-160	0,000261	0,000396	240°-270°
								160-200	0,000310	0,000245	210°240°

20	703903,8486	1,286±0,185	8,28	4,8	31,2	31,2	360	0-40	0,766811	2,599594	330°-30°
								40-80	0,000223	0,000316	330°-30°
								80-120	0,000090	0,000070	30°-60°, 240°-270°
								120-160	0,000131	0,000156	30°-60°
								160-200	0,000148	0,000152	30°-60°, 120°-150°, 300°330°
21	977873,8798	1,04±0,2	6,63	4,9	-	-	-	0-40	0,000117	0,000074	210°-240°
								40-80	NaN	NaN	NaN
								80-120	NaN	NaN	NaN
								120-160	NaN	NaN	NaN
								160-200	NaN	NaN	NaN

References

Almeida, F. F. M. de, Neves B. B. de B. and Carneiro, C. D. R. 2000. The origin and evolution of the South American Platform. Earth Science Reviews, 50, p. 77-111.

Bilek, S.L., 2009. Seismicity along the South American subduction zone: Review of large earthquakes, tsunamis, and subduction zone complexity, Tectonophysics, Volume 495, Issues 1–2, p. 2–14.

Cardona, C., Salcedo, E. de J., Mora, H. 2005. Caracterización sismotectónica y geodinámica de la fuente sismogénica de murindó – colombia. Boletín de Geología [online] 2005, 27 (Enero-Junio): Available in: ISSN 0120-0283

CCGM/CGMW. 2009. Mapa Geológico del Mundo a escala 1:50 0 000 000. ISBN 978-2-917310-03-8.

Chen, P.-F., Bina, C. R., and Okal E. A. 2001. Variations in slab dip along the subducting Nazca Plate, as related to stresspatterns and moment release of intermediate-depth seismicity and to surface volcanism, Geochem. Geophys.Geosyst., 2, 10.1029/2001GC000153.

Corredor, F. 2003. Seismic strain rates and distributed continental deformation in the northern Andes and three-dimensional seismotectonics of northwestern South America. Tectonophysics 372.

Gutscher M. A., Spakman, W., Bijwaard, H., Engdahl E. R. 2000. Geodynamics of flat subduction: Seismicity and tomographic constrains from the Andean margin. Tectonics, vol.19, No.5, 814-833.

Hainzl, S., Enescu, B., Cocco, M., Woessner, J., Catalli, F., Wang, R. and Roth, F. 2009.Aftershock modeling based on uncertain stress calculations, Journal of Geophysical Research, vol. 114, 2009. p. 6–7

Holt, W.E., Ni, J.F., Wallace, T.C., Haines, A.J. 1991. The active tectonics of the Eastern Himalayan Syntaxis and surrounding regions. J. Geophys. Res. 96, 14595– 14632.

International Seismological Center (ISC). 2010. Online Bulletin. http://www.isc.ac.uk/iscbulletin/. r. Thatcham, UK. Vol. 4 Issue 1-6.

Marques, F.O., Nikolaeva, K., Assumpcao M., Gerya, T. V., Bezerra F. H. R., Nascimento A. F. and Ferreira J. M. 2013. Testing the influence of far-field topographic forcing on subduction initiation at a passive margin.Tectonophysics, 608, p. 2-5.

Müller, R. D. and Landgrebe, C. W. 2012. The link between great earthquakes and the subduction of oceanic fracture zones. Solid Earth, 3, p. 447–465, doi:10.5194/se-3-447-2012.

Ramos, V. A., 1999. Plate tectonic setting of the Andean Cordillera. Episodes, Vol. 22, No. 3, 183-190.

Ramos, V.A. and Folguera, A. 2009. Andean flat-slab subduction through time. The Geological Society of London, Special Publications, 327, 31-54.

Ramos, V.A., 2009. The tectonic regime along the Andes: Present – day and Mesozoic regimes. Geol. J. 45: 2-25.

Rhea, S., Hayes, G., Villaseñor, A., Furlong, K. P., Tarr, A.C. and Benz, H. 2010. Seismicity of the Nazca Plate and South America: U.S. Geological Survey Open-File Report, scale 1:12,000,000.

Salazar, J., and Vargas, C. 2015. Fractal Dimension and Seismotectonic Deformation Rates along an inter-plate setting: Seismic Regime along the Caribbean Plate Boundary Zone. Submitted to American Association of Petroleum Geologists (AAPG).

Sanchez L. and Seitz M., DGFI Report No. 87 - Recent activities of the IGS Regional Network Associate Analysis Centre for SIRGAS, 2011

Shen, Z.K., Jackson, D.D. and Ge, B.X. 1996. Crustal deformation across and beyond the Los Angeles basin from geodetic measurements, Journal of Geophysical Research, Vol. 101, 27, 957-27, 980.

Stein, S. and Wysession, M. 2013.An introduction to Seismology, earthquakes, and earth structure. Ch1. 9-4, Ch5. 286-290 and 308-325. ISBN 0-86542-078-5.

Storchak, D. A., Giacomo, D. D., Bondár, I., Harris, J., Engdahl, E. R., Lee, W. H. K., Villaseñor, A., Bormann, P. and Ferrari, G. 2012. ISC-GEM Global Instrumental Earthquake Catalogue (1900-2009), GEM Technical Report 2012-01 v1.0.0, 128 PP., GEM Foundation, Pavia, doi: 10.13117/GEM.GEGD.TR2012.01.

Swis Re Foundation and the Global Earthquake Model (GEM) Foundation. 2014. South America Integrated Risk Assessment.

Teza, G., Pesci, A. and Galgaro, A. 2008.Grid_strain and grid_strain3: Software packages for strain field computation in 2D and 3D environments. Computers & Geosciences, 34, 1142-1153.
Van der, M., Julia, J., Assumpcao, M. 2013.Gravity derived Moho for South America. Tectonophysics, 609, 456-467.

Van Stiphout, T., Zhuang, J. and Marsan, D. 2012. Seismicity declustering, Community Online Resource for Statistical Seismicity Analysis, doi: 10.5078/corssa-52382934. Available at http://www.corssa.org, p. 9–12.

Vergnolle, M., Walpersdorf, A., Kostoglodov, V., Tregoning, P., Santiago, J. A., Cotte, N. and Franco. S. I. 2010. Slow slip events in Mexico revised from the processing of 11 year GPS observations, J. Geophys. Res., 115.

Zuñiga, F.R., Reyners, M. and Villamor, P. 2005. Temporal variations of the earthquake data in the catalogue of seismicity of New Zealand. Bulletin of the New Zealand Society for earthquake Engineering, vol. 38, No. 2.